Quantification of Vertical Profiles of Cross-Shore, Swash-Zone Flow in the Near Bed Region Using Particle Image Velocimetry

by

Douglas Krafft

A thesis submitted to the Faculty of the University of Delaware in partial fulfillment of the requirements for the degree of Honors Degree in Civil Engineering with Distinction

Spring 2015

© 2015 Douglas Krafft
All Rights Reserved

Quantification of Vertical Profiles of Cross-Shore, Swash-Zone Flow in the Near Bed Region Using Particle Image Velocimetry

by

Douglas Krafft

Approved: _____

Jack A. Puleo, Ph.D.
Professor in charge of thesis on behalf of the Advisory Committee

Approved: _____

Tian Jian Hsu, Ph.D.
Committee member from the Department of Civil and Environmental Engineering

Approved: _____

Joshua Zide, Ph.D.
Committee member from the Board of Senior Thesis Readers

Approved: _____

Michael Arnold, Ph.D.
Directory, University Honors Program

ACKNOWLEDGMENTS

I would like to thank everyone who helped in either of the two experiments, or the data analysis process. In particular I am grateful for the extensive contributions of time from Professor Jack Puleo and José Carlos Pintado Patiño which made the entire experience possible.

I would also like to thank the Undergraduate Research Program for their award of Undergraduate Research Conference and Travel Expense funding. This facilitated the inclusion of data from the experiment at Oregon State University.

TABLE OF CONTENTS

LIST OF FIGURES vi
ABSTRACT ix

1 Introduction 1

1.1 Significance 1

2 Particle Image Velocimetry 5

2.1 The Concept of Particle Imaging Velocimetry 5
2.2 PIV Algorithm 6
2.3 Cross Shore Swash-zone PIV 8

3 Methods 9

3.1 Instrumentation 9

3.1.1 The Camera System 9

3.1.1.1 Camera system components 9
3.1.1.2 Camera system placement and settings 13

3.1.2 The Vectrino II Profiling Velocimeter 17

3.2 Experiments 18

3.2.1 The Experiment at the University of Delaware 19
3.2.2 Sand BAR SEDiment Transport Experiment 20

3.3 Data Analysis 22

3.3.1 Image Rectification 22
3.3.2 The Application of Particle Image Velocimetry 25
3.3.3 Vector Correction 26

3.3.3.1 Vectrino II Velocity Correction 26
3.3.3.2 PIV Output Correction 27

3.3.4 Data Alignment 30

3.3.4.1 Temporal Alignment 30
3.3.4.2 Spatial Alignment 31

4 Results and Discussion 33

4.1 Discussion of Results from the Experiment in the CACR 33

4.1.1 Velocity Time Series from the Experiment in the CACR 33
4.1.2 Error 35
4.1.3 Vertical Velocity Profiles from the CACR 39

4.2 Results from BARSED 46

4.2.1 BARSED Velocity Time Series 46
4.2.2 Error 48
4.2.3 Vertical Velocity Profiles from BARSED 50

5 Conclusion 55

REFERENCES 57

VARIABLES 58

LIST OF FIGURES

Figure 1 Coastal regions diagram (http://www.fhwa.dot.gov/engineering/hydraulics/hydrology/hec25c7.cfm) 2

Figure 2. Graphical representation of PIV. 5

Figure 3. Underwater camera housing wiring diagram, 1. System attached to bulkhead and cable 1, controls lighting and grounds system, 2. System attached to bulkhead and cable 2, controls lens and supplies power to camera, 3. Ethernet cable attached to bulkhead and cable 3, carries camera data. 10

Figure 4. Complete camera system wiring diagram: I. lighting system: lights, 2 manual potentiometers; II. lens control system: zoom lens, lens control; III. camera system: camera, high performance computer, Gigabit Ethernet data transmission, camera power 11

Figure 5. Camera housing on tripod 12

Figure 6. Recording and controlling section of the camera system. A. High performance computer, B. Variable Power Supply for the Camera, C. Lens controller, D. Manual Potentiometers 13

Figure 7 Conceptual plan view of camera deployment observing uprush 14

Figure 8 Conceptual drawing of the field of view for the camera 14

Figure 9. Conceptual drawing of a vertical alongshore view of the camera position .. 16

Figure 10. Conceptual drawing of a Vectrino II profiling velocimeter. (http://www.nortek-as.com/lib/brochures/vectrino-ii) 18

Figure 11. The counterweight and gate in the Precision flume at the CACR 19

Figure 12. BARSED swash experiment configuration, A. The camera housing, B. The Camera control system 21

Figure 13. Calibration images for BARSED (top) and the experiment in the CACR (bottom) with the ruler lying parallel to the sediment slope. 24

Figure 14. Velocity time series for a single Vectrino II bin, raw Vectrino II velocity (top), corrected Vectrino II velocity (bottom) 27

Figure 15. An example of the spurious vector removal process results for the plot of velocity against time for a single elevation, raw data (top), retained data (bottom). 28

Figure 16. A plot of the approximate acceleration against time at a single elevation.. 29

Figure 17. A frame collected before the first run (CACR experiment), indicating the cross-shore location of the Vectrino II. 31

Figure 18. Time Series comparison between the velocities measured by the Vectrino II (red), and those from PIV (blue) from 18 to 2 mm from the initial bed level. 34

Figure 19. Relative error as a function of elevation, for all interrogation window sizes from the experiment in the CACR. 36

Figure 20. Relative error for the larger three interrogation window sizes from the experiment at the in the CACR, as a function of elevation. 37

Figure 21. Histograms of the relative error for the velocities at elevations of 18, 10, 4 and 2 mm 38

Figure 22. Water depth (top) and image frames from the uprush in the CACR experiment, PIV (blue), Vectrino II (red), 1 m/s scale vector (cyan)..... 40

Figure 23. Water depth (top) and image frames from backwash, before significant sediment mobilization, PIV (blue), Vectrino II (red), 1 m/s scale vector (cyan) 43

Figure 24. Water depth (top) and image frames of late backwash from the experiment in the CACR, PIV (blue), Vectrino II (red), 1 m/s scale vector (cyan) 45

Figure 25. Comparisons of Velocities at 11, 7, and 4 mm above the bed plotted against time, PIV (blue), Vectrino II (red) 47

Figure 26. Relative Error between PIV and Vectrino II data from BARSED 48

Figure 27. Relative error histogram for 12, 9, and 5 mm velocities at BARSED 49

Figure 28. Velocity time series (top) image frames for the first backwash considered from BARSED, PIV (blue), Vectrino II (red), 1 m/s scale vector (cyan) 50

Figure 29. Velocity time series (top) image frames for the initial uprush considered from BARSED, PIV (blue), Vectrino II (red), 1 m/s scale vector (cyan) 51

Figure 30. Velocity time series (top) image frames for the uprush considered from BARSED, PIV (blue), Vectrino II (red), 1 m/s scale vector (cyan) 53

Figure 31. Velocity time series (top) image frames for the second backwash considered from BARSED, PIV (blue), Vectrino II (red), 1 m/s scale vector (cyan) 54

ABSTRACT

Erosion is a very real problem facing many beaches. Sediment transport in one particular coastal region, the swash zone, is particularly important for understanding coastal erosion. Sediment transport cannot be measured directly, so velocity and sediment concentration are used. Current meters are unable to measure the entire duration the swash event, and cannot measure sheet flow. Sheet flow is a particularly high concentration, near-bed mode of sediment transport, which is an important part of swash-zone sediment transport. This senior thesis examines the capability of particle image velocimetry (PIV) to quantify near-bed, cross-shore vertical velocity profiles, in the swash zone. Determining velocities in temporal gaps in current meter data, and sheet flow are two particular goals. Data from two laboratory flume based swash zone studies were considered. The first experiment, in the Center for Applied Coastal Research scale flume, involved a dam-break swash event over a slope of coarse sediment in a scale flume. The second involved a series of swash events from waves generated by a wave-maker over a slope of finer grained sediment in the O.H. Hinsdale large wave flume. Camera imagery was processed with PIV to develop vertical velocity profiles. These profiles were compared with velocity measurements from a collocated current meter. The results indicate that PIV is capable of determining accurate velocity profiles, velocity profiles through sheet flow, and velocities earlier and later in a swash event than the collocated current meter.

Chapter 1

Introduction

1.1 Significance

Coastal erosion threatens a large number of the world's beaches. The coast is a culturally and economically important region. Furthermore, the coast is a natural wonder, worth preserving for future generations. The negative consequences of coastal erosion make understanding sediment transport in the coastal environment especially important.

The beach profile can be divided into the nearshore and offshore zones. The primary interest of this work is sediment transport in the nearshore zone. The nearshore zone can be divided into two main regions: the surf zone, and the swash zone (Figure 1). Waves move from the offshore towards the beach, become unstable, break, and dissipate energy. Near the shoreline a collapsed bore travels up the beach as uprush and returns as backwash in the swash zone. The swash zone is the most landward section, defined as the area covered by uprush and exposed by backwash. The swash zone is the region which predominantly interacts with the emerged portion of the beach and most directly impacts the most widely used region of the beach. Swash-zone flows are shallow, fast, and highly turbulent, with high sediment concentrations. As a result, swash-zone sediment transport plays a crucial role in coastal erosion.

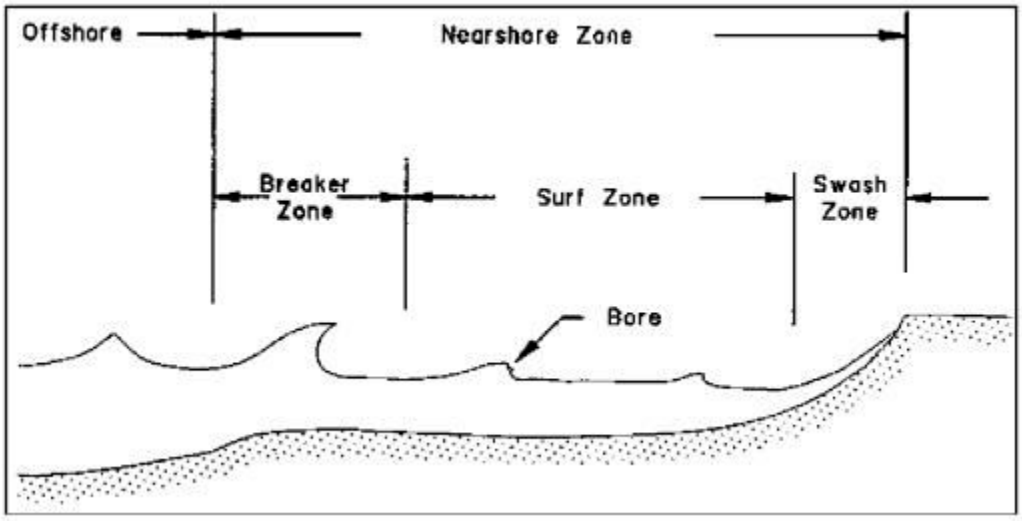

Figure 1 Coastal regions diagram (http://www.fhwa.dot.gov/engineering/hydraulics/hydrology/hec25c7.cfm)

Sediment transport can be divided into three modes: bed load, suspended load, and sheet flow. Sediment grains moving in the bed load are lowest in the water column. Their motion is characterized by extensive grain to grain interactions (Komar, 1978). Suspended load moves sediment higher in the water column, where particles are kept in suspension by turbulence (Komar, 1978). Sheet flow occurs in the lower region of the water column, and moves high concentrations of sediment. This sediment and water mixture is a predominantly planar subsection of the swash flow with particularly high concentration. It extends several millimeters to several centimeters above the immobile bed, and is mobilized by high shear stress.

The initiation of sheet flow can be described by the Shields number θ

$$\theta = \frac{\tau_b}{(\rho_f - \rho_s) g d} \quad (1)$$

where τ_b is bed shear stress, ρ_f is fluid density, ρ_s is sediment density, g is gravitational acceleration, and d is the grain diameter. Sheet flow mobilizes at θ greater than 0.8 -1.0. As its concentration is so high, sheet flow moves a substantial quantity of sediment in spite of its shallow depth, contributing significantly to the rapid morphologic changes in the swash zone.

One of the primary interests in the study of erosion is sediment flux, which is defined by concentration and velocity. Sediment flux cannot be measured directly, so a combination of sediment concentration and velocity measurements must be used. With an array of sensors, sediment concentration can be determined over the full swash-zone water column during the entire swash event. Velocity measurement capabilities are less complete. The two main types of velocity sensors are acoustic and electromagnetic. Neither is able to measure the full spatial and temporal range of velocities. They are unable to measure the entire duration of a swash event, and are unable to measure sheet flow velocity. Both sensors have difficulties measuring the velocity in high concentration flows. Acoustic sensors rely on the return of a signal. These signals can become complex with high concentrations of moving sediment or bubbles. Swash flows are often strongly turbulent, and may contain significant bubbles and high sediment concentrations. The most significant occurrences of the conditions are during the initial uprush. Neither sensor type can measure a velocity profile over the beginning of uprush. Most sensors also only function in water. This becomes a problematic requirement in the swash-zone, where sensors will quite likely be

intermittently submerged or exposed because of their size and required elevations above the fixed bed. As result later velocities in later backwash cannot be measured. The incomplete time series and lack of reliable sheet flow velocities present gaps in the ability to quantify sediment flux.

This senior thesis examines the ability to provide velocities using PIV for aspects of swash event where current meters cannot measure. A particular focus is the capability of PIV to determine velocity profiles through the sheet flow layer, during the onset of uprush, and after the swash thins. The most promising of these scenarios is the high concentration environment of sheet flow. Unlike acoustic or electromagnetic velocity sensors, PIV performs well for high concentration flows. This largely motivates the application of PIV to determine vertically resolved velocity profiles in the swash-zone. Imagery analyzed with PIV was collocated with a Vectrino II Profiler which measured velocity in the lower water column concurrently. To determine their accuracy, the velocities obtained through PIV were compared with data from the Vectrino II.

Chapter 2

Particle Image Velocimetry

2.1 The Concept of Particle Imaging Velocimetry

PIV is a technique that determines velocity by comparing images separated by known time steps. Comparing the location of a pattern from the first image with the location of the same pattern in the second image determines a displacement, ΔX, as shown in Figure 2.

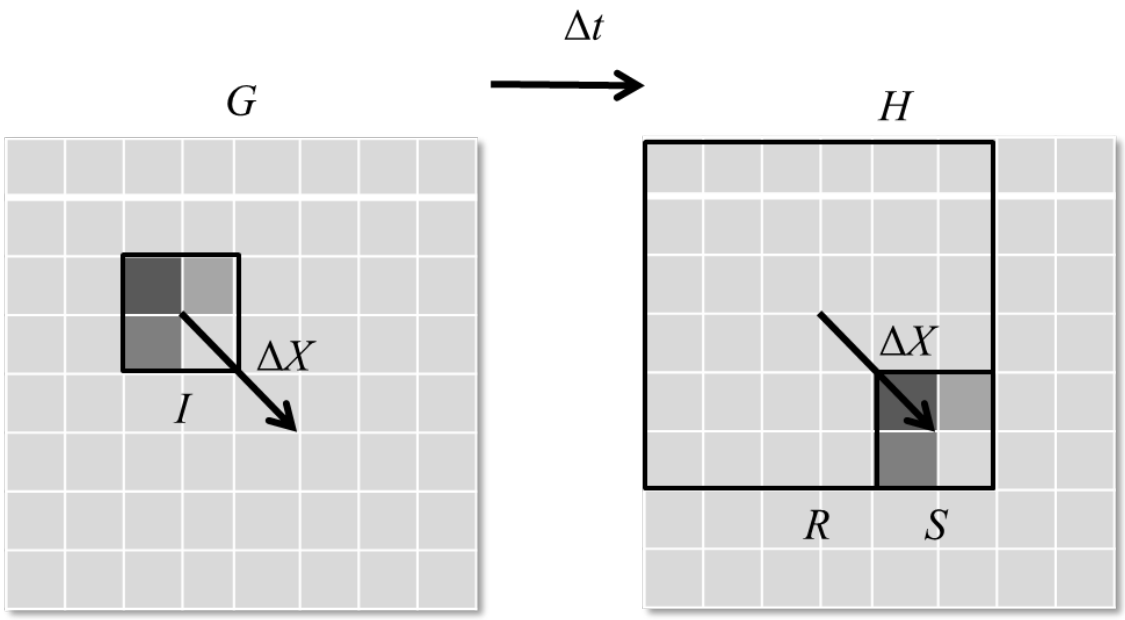

Figure 2. Graphical representation of PIV.

PIV compares subregions of the two images *G* and *H*. An interrogation window *I*, of the size $2i+1$ x $2i+1$ pixels, is selected and centered on a particular grid point in *G*. Over the time step Δt the pattern translates ΔX. A search window *S*, also of size $2i+1$ x $2i+1$ pixels, is centered over the translation of *I* in *H*. The distance between the center of *I* and the center of *S* defines ΔX. *R* is the search region, which is the area where *S* is searched for based on expectations of the maximum velocity. The local velocity of *I* is determined by dividing ΔX by Δt.

2.2 PIV Algorithm

The PIV algorithms used in this work were written in MATLAB (original code by Professor Jack Puleo, modified by Douglas Krafft). Monochromatic images are expressed in MATLAB as 2 dimensional matrices of pixel intensities from 0 to 255. A grid of points is considered within *G*, with an *I* centered around each point. A search region *R* is also centered about every point in the grid for *H*. The grid considered here applies a uniform spacing in the horizontal and vertical directions.

The same grid of points is applied over the entire sample, so only a general knowledge of the images may guide the selection of the individual interrogation windows. *I* is large enough to capture a unique and recognizable pattern at any grid point within the region of interest. Locating the texture from *I* within *R* requires the comparison of two identically sized images. *I*, the subset of *G*, is compared with *S*, the subset of *H*. *S* must also be defined as $2i+1$ to be the same size as *I*. Because the comparison is between *I* and one equally sized *S*, an *S* must be generated for every possibility considered. Search windows are generated to cover every pixel in *R*.

For comparing *I* to S, there are a wide range of correlation equations that can be applied. These include cross correlation, error correlation, minimum quadratic

difference and minimum absolute difference. This thesis uses the error correlation method. Using error correlation provides similar results to cross-correlation with lower computation times, and without biasing higher pixel intensities (Roth et al., 1995; Holland et al., 2001). In error correlation the correlation value for each specific x_m, z_n pair contained in the search region is calculated as

$$\Phi(x_m, z_n) = 1 - \frac{\sum_{j=1}^{2i+1}\sum_{k=1}^{2i+1}|S(j,k)-I(j,k)|}{\sum_{j=1}^{2i+1}\sum_{k=1}^{2i+1}S(j,k)+I(j,k)}. \quad (2)$$

Where i is the interrogation half-length; j and k are counters, $S(j,k)$ is the intensity of the j, k pixel in the search window S for x_m, z_n, and is the $I(j,k)$ is the intensity of the j, k pixel in the interrogation window I.

A Φ is calculated for every x_m, z_n combination in R. Within the matrix of Φ values, the maximum is selected. The difference between the original x, z and the x_m, z_n selected provides ΔX, of components Δx which is m, and Δz which is n. Dividing by the known time difference, Δt, between frames G and H, provides the velocities u and w for I.

As with most correlation equations, error correlation relies on simple image subtractions. Image subtractions subtract the pixel values at each matrix location between the two images. This makes the comparison entirely orientation dependent. The importance of the location of the pixels within the pattern in I mean that any deformation of I over Δt will mean that an S cannot be found to perfectly match I. Any rotation of I over Δt will result in the absence of a perfectly matching S. Too much rotation, even without deformation will prevent the matching of I to the correct S. The method assumes a linear translation of non-deforming pattern for perfect matches of Φ=1. The severity of the deviations from this assumption determines the effectiveness of correlation. A certain level of error is acceptable, and even inherent. As long as the

true S and I are still the most similar, this error is minimized by choosing the highest Φ value.

2.3 Cross Shore Swash-zone PIV

This application of PIV aims to quantify vertical profiles of cross shore near bed velocity. Grain boundaries of sediment clusters are used as the patterns matched between images. Sediment grains mobilized by the swash event will travel with the flow and thus perpendicular to the camera. Using a column of interrogation windows beginning in the immobile bed, and extending into the flow, PIV provides a vertical profile of velocity with a chance of resolving the transition from zero velocity through sheet flow

Chapter 3

Methods

3.1 Instrumentation

The primary interest was determining velocities. In particular, the focus was using the Vectrino II Profiling Velocimeter and Particle Image Velocimetry.

3.1.1 The Camera System

3.1.1.1 Camera system components

PIV has the strongest results with clear, well contrasted, and high frequency imagery. The camera system used in this experiment was high frame rate and low exposure time, with particularly applicable focus and zoom, as well as powerful illumination. The camera was a Teledyne Dalsa Genie HM. It captures time-sequenced 640 by 480 pixel imagery at a rate of 301 frames per second. The camera is used in conjunction with the Norpix Digital Video Camera Recording software StreamPix 6, where the exposure time and several other camera settings may be adjusted while capturing imagery, which facilitates optimizing settings. The system was equipped with a Computar remote control lens. The zoom and focus could also be adjusted without removing the camera from its housing, in the environment in which it operated. The camera was connected to a high performance computer which was selected to accommodate the high frame rate.

The camera system was deployed in a housing with underwater capabilities. The various wirings for controlling the camera system were passed out of the housing through three bulkheads, and sent to the computer and controls through three cables. The internal wiring diagrams of the Camera housing, as well as the overarching wiring diagrams are provided in Figures 3 and 4.

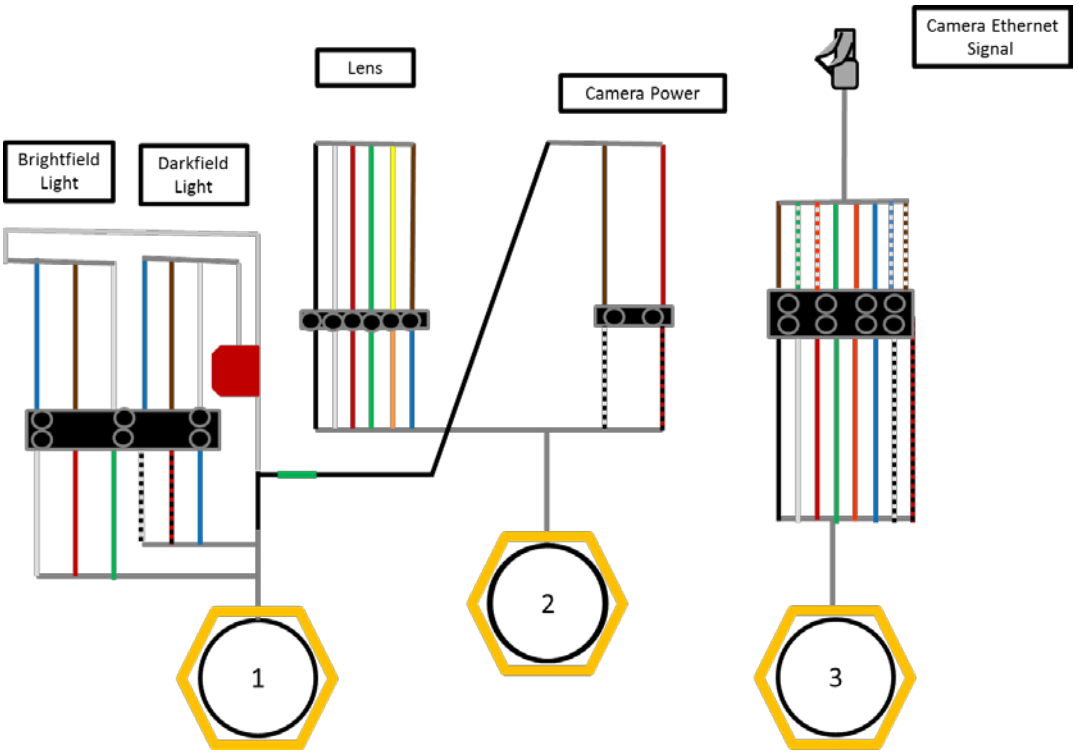

Figure 3. Underwater camera housing wiring diagram, 1. System attached to bulkhead and cable 1, controls lighting and grounds system, 2. System attached to bulkhead and cable 2, controls lens and supplies power to camera, 3. Ethernet cable attached to bulkhead and cable 3, carries camera data.

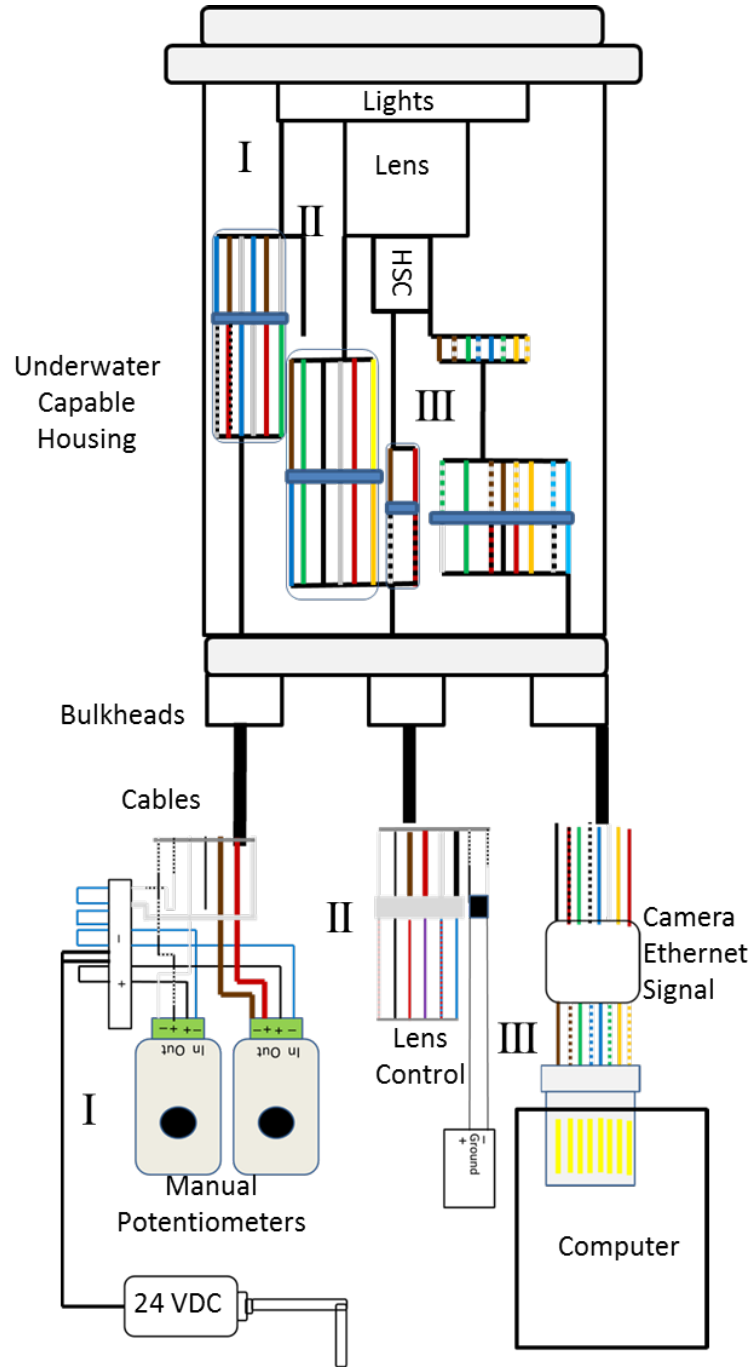

Figure 4. Complete camera system wiring diagram: I. lighting system: lights, 2 manual potentiometers; II. lens control system: zoom lens, lens control; III. camera system: camera, high performance computer, Gigabit Ethernet data transmission, camera power

The operation of this camera system relies on many connections (Figure 3, Figure 4). These were made with crimp terminal connectors, each unique within the system so as to reduce the potential for incorrect wiring in future deployments. Being able to control the zoom, focus, exposure time, and lighting, after the camera has been deployed forms a substantially more robust data collection system. These capabilities require the complex wiring layout. Cables connect the camera to the computer, lens controller, and manual potentiometer. The two ends of the system are shown in Figures 5 and 6.

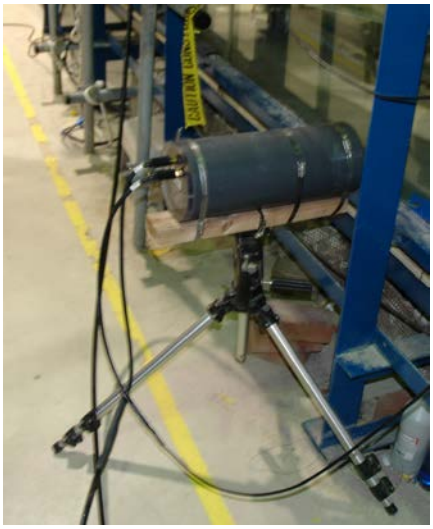

Figure 5. Camera housing on tripod

Figure 6. Recording and controlling section of the camera system. A. High performance computer, B. Variable Power Supply for the Camera, C. Lens controller, D. Manual Potentiometers

3.1.1.2 Camera system placement and settings

In this thesis a camera faces perpendicular to the swash flow.

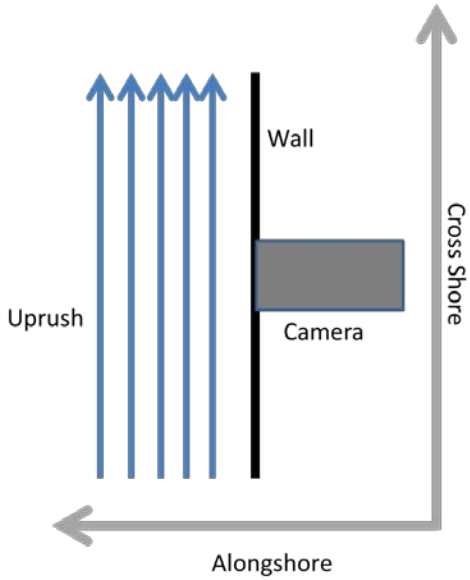

Figure 7 Conceptual plan view of camera deployment observing uprush

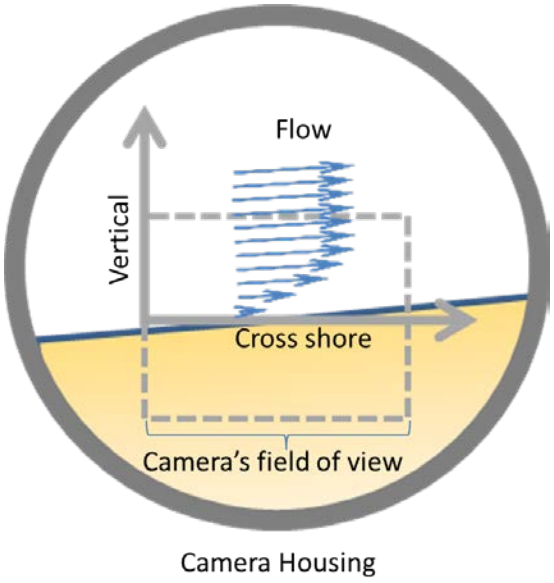

Figure 8 Conceptual drawing of the field of view for the camera

As Figures 7 and 8 show, the Camera looks alongshore to view vertical profiles cross shore flow. In the coordinate system used here, and throughout this senior thesis, the vertical axis matches the standard directions of up and down. The horizontal plane is divided into two components. The cross shore direction is the horizontal component of the vector normal to a beach contour. In this thesis, the cross shore may be expressed more simply as the horizontal component of the primary direction of the swash flow. The alongshore direction is the horizontal direction normal to the cross shore axis. In this thesis the alongshore will be horizontal and perpendicular to the flow. When applied in this fashion, Particle Image Velocimetry can determine cross shore and vertical velocities.

The camera was positioned to best capture a vertical profile of cross shore velocities which extend through sheet flow and into the immobile bed. The camera was placed partially below the sediment (Figure 8, Figure 9) to ensure that the boundary was observed and continued to be in the field of view during sediment transport.

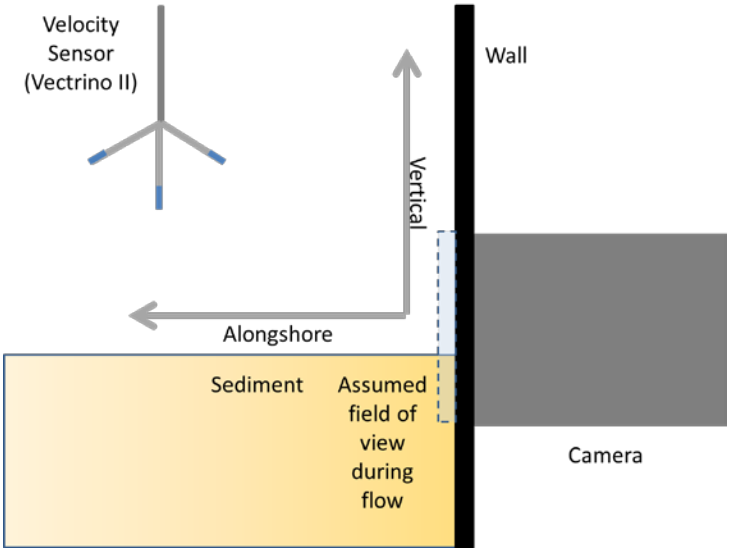

Figure 9. Conceptual drawing of a vertical alongshore view of the camera position

Capturing the boundary of the sediment bed is important to ensure that a velocity profile will extend to a point of zero velocity, observing whatever sheet flow might occur. A field of view on the order of 50 by 70 mm was used.

PIV relies on matching images of moving clusters of sediment grains, so the image clarity is important. Better resolved clusters are easier to match between frames; therefore, low exposure times are important. Motion introduces distortions of sediment clusters in the imagery. In an image the moving sediment grains will “smear” to cover the locations they occupied during the exposure time. Longer exposures correspond directly with more severe distortions. Because this work focused on the swash zone, particularly sheet flow and the initial uprush, minimizing distortions is especially relevant. Sheet flow and the beginning of uprush have some of the highest sediment concentrations. For high concentration flows, sediment grains will be densely spaced. Distortions could cause the sediment grains to “bleed” into one another in fast, high

concentration flows. The contrast of the sediment grain cluster boundaries should be kept intact for optimal PIV results. In order to mitigate distortions the experiments used an exposure time of 1 ms.

The lighting is also important for the camera system. PIV matches patterns, so for meaningful results these patterns should be clusters of sediment, not ambient light. As a result, the camera needs illumination strong enough to overpower other light sources which the field of view is exposed to. If a shadow is the most distinct pattern recorded for a grid point, that location will only yield erroneous data. The lighting supplied must also overcome the effect of drastically lowering the exposure time, to keep sediment grains well illuminated.

3.1.2 The Vectrino II Profiling Velocimeter

The Vectrino II makes use of Coherent Doppler processing to determine a vertical velocity profile (http://www.nortek-as.com/lib/brochures/vectrino-ii). Put simply, the Vectrino II measures the response times of several acoustic beams, and converts those into a column of three-dimensional velocity vectors. The Vectrino II and its acoustic beams are presented in Figure 10.

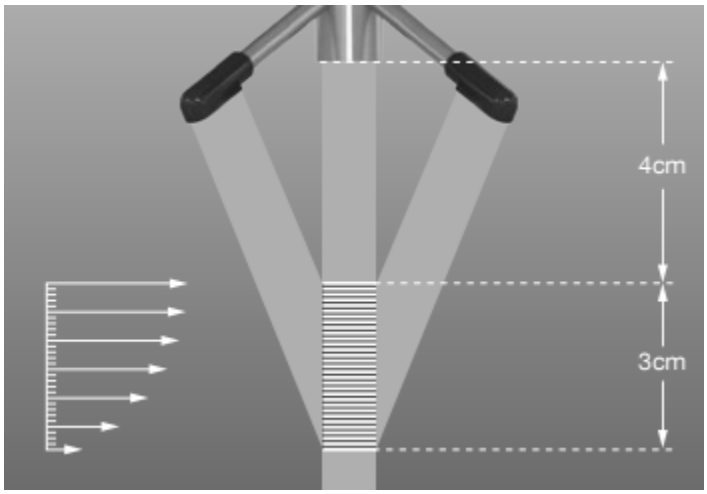

Figure 10. Conceptual drawing of a Vectrino II profiling velocimeter. (http://www.nortek-as.com/lib/brochures/vectrino-ii)

With the beams shown in Figure 10, the Vectrino II measures the response time of the Coherent Doppler signals, and the correlation of the return signal. These are converted into 3D velocity measurements over the 30 mm from 40 mm to 70 mm from the sensing head of the Vectrino II. Another output of the Vectrino II is the amplitude of a beam pointed straight down and used to identify the bed location. The outputs which most concern this work are the velocity measurements in the x and z directions. These are two-dimensional velocity vectors at 31 vertically aligned points, sampled at 100 Hz. The Vectrino II supplies a reliable velocity profile, provided corrections have been implemented for the readings from below the bed. This profile is taken as the groundtruth velocity in the water column.

3.2 Experiments

This senior thesis examines the results from two experiments on swash-zone flow over a slope of sediment. Important parameters such as sediment size, location

within the swash-zone and wave forcing were varied between the experiments. The same key instrumentation was used in both, collecting wave height measurements, vertical velocity profile measurements, and sediment transport imagery.

3.2.1 The Experiment at the University of Delaware

One data set which this thesis examines is from an experiment conducted at the University of Delaware in the Center for Applied Coastal Research (CACR) Precision Flume. The study examined a single swash event over a planar slope of sediment. The swash event was simulated by a dam-break. To generate the wave for the swash event, a rotating counterweight was released to quickly lift the gate from the reservoir (Figure 11).

Figure 11. The counterweight and gate in the Precision flume at the CACR

Before the first run the mean slope was set to 1 on 7. Angular sediment of an average grain diameter on the order of 1 mm formed the planar slope. While 1 mm is relatively coarse grain diameter, the size was selected to provide the most useful imagery for PIV. The larger ratio of pixels to grains in the imagery resulted in more distinct patterns, which were more likely to be matched by the PIV algorithm. The large grain diameter also reduced the suspended load which may have shortened the vertical and temporal range over which PIV provides accurate correlations.

An ultrasonic distance meter (UDM) measured the water level, a Vectrino II measured the flow velocity, and the camera collected imagery at the cross-shore location of the Vectrino II. The camera imaged a field of view of 87.6 by 65.7 mm, so the spatial region of the swash considered is small. As a result, the cross-shore position of the camera is particularly important. In order to capture the most violent and longest lived swash event the camera was located 0.9 m from the toe of the slope. The Vectrino II was approximately 60 mm above the bed. Cables were run from the Camera and Vectrino II back to tables with computers collecting data and keeping them connected to the GPS-updated time server (Figure 6).

3.2.2 Sand BAR SEDiment Transport Experiment

The other data set was collected during the sandBAR SEDiment transport experiment (BARSED). BARSED was conducted at Oregon State University, in the O.H. Hinsdale large wave flume. The flume contained a wave-maker at the far seaward end, a ramp of concrete leading up to the sandbar, a trough, and a farther onshore section at a 1 on 12 slope. The flume also had a swash-zone addition. A wooden wall extended from the inner surf zone to the landward end of the flume. The added wall was spaced approximately 0.6 m from the flume wall. The space between

these two walls was filled with sediment to a depth of 150 mm. The depth was subject to change over the course of the experiment. A window allowed the camera to observe the flow between the wooden wall and the nearer flume wall. As the Vectrino II was continuously submerged, the measurement locations were just seaward of the swash zone. The Camera position is shown in Figure 12.

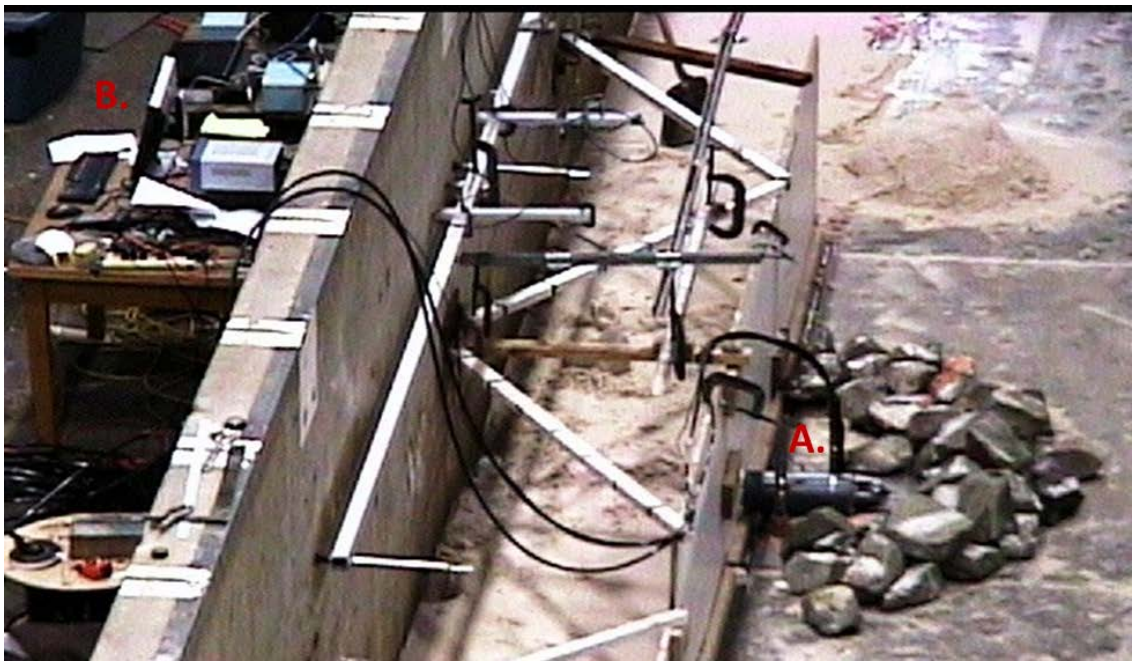

Figure 12. BARSED swash experiment configuration, A. The camera housing, B. The Camera control system

The camera housing was placed on the far side of the wooden wall to minimize flow disturbance (Figure 12, A). The PIV analysis used in this work focused on the x-z plane particularly near to the housing front face plate, so particular care was given to minimizing the disturbance at the camera housing face plate. The observation was sufficiently landward of the start of the wooden wall, to minimize the impact on the

flow in the channel. The camera housing was levelled to the horizontal and vertical axes.

A Vectrino II was positioned at the cross-shore location of the camera. An ultrasonic wave gauge was also placed to record water surface elevation at the same cross-shore location. Cables were passed over the flume walls. The cables terminated at a table along the flume edge where two computers collected the camera image sequences and Vectrino II data. The lens controls, manual potentiometers, and computer were also connected to the cables passed up from the camera (Figure 12, B). The camera and Vectrino II data were kept on the same reference time by the time server connected to both computers.

Due to practical considerations for the camera system, image sequences were limited to 20,000 frames. The necessity of writing the entire image sequence to RAM before saving required the possible length of a recording to be limited. When the computer runs low on RAM, StreamPix 6 cannot access RAM fast enough to process the data when it arrives at 301 Hz, so it automatically reduces the frame-rate when it detects that the RAM is too low. After some preliminary testing, the duration of 20,000 images or 66.5 seconds was chosen to ensure that the framerate did not drop unexpectedly.

3.3 Data Analysis

3.3.1 Image Rectification

The rectification of the camera imagery to real world coordinates used several simplifications and observed measurements. As a true rectification of the axes between the image and the real world coordinates fell outside of the scope of this

thesis, the camera was level along all three axes. The observed swash event is also assumed to be flowing only in the cross-shore and vertical directions. Using the particularly low exposure time of 1.0 ms, a spacer ring between the camera and the lens, and a strong light, the alongshore depth of the field of view is limited. Using this limitation, patterns observed are assumed to be close enough to the location of the scale for it to apply. To strengthen this assumption further, the cross-shore vertical plane considered is in the immediate proximity of the window between the camera and the flow. This position limits the possibility of textures in a different vertical plane moving between the camera and the assumed vertical plane.

The scale of pixels to meters was determined by imaging a ruler placed in the field of view. Using the images in Figure 14 the distances between two sets of cm marks in the images were recorded. The average of the distances was taken, divided by ten and inverted to find the pixel to mm scale. A pixel represents 0.1369 mm for the experiment in the CACR, and 0.1053 mm at BARSED. Therefore a field of view of 67.4 by 50.5 mm was used for BARSED and 87.6 by 65.7 mm for the experiment in the CACR.

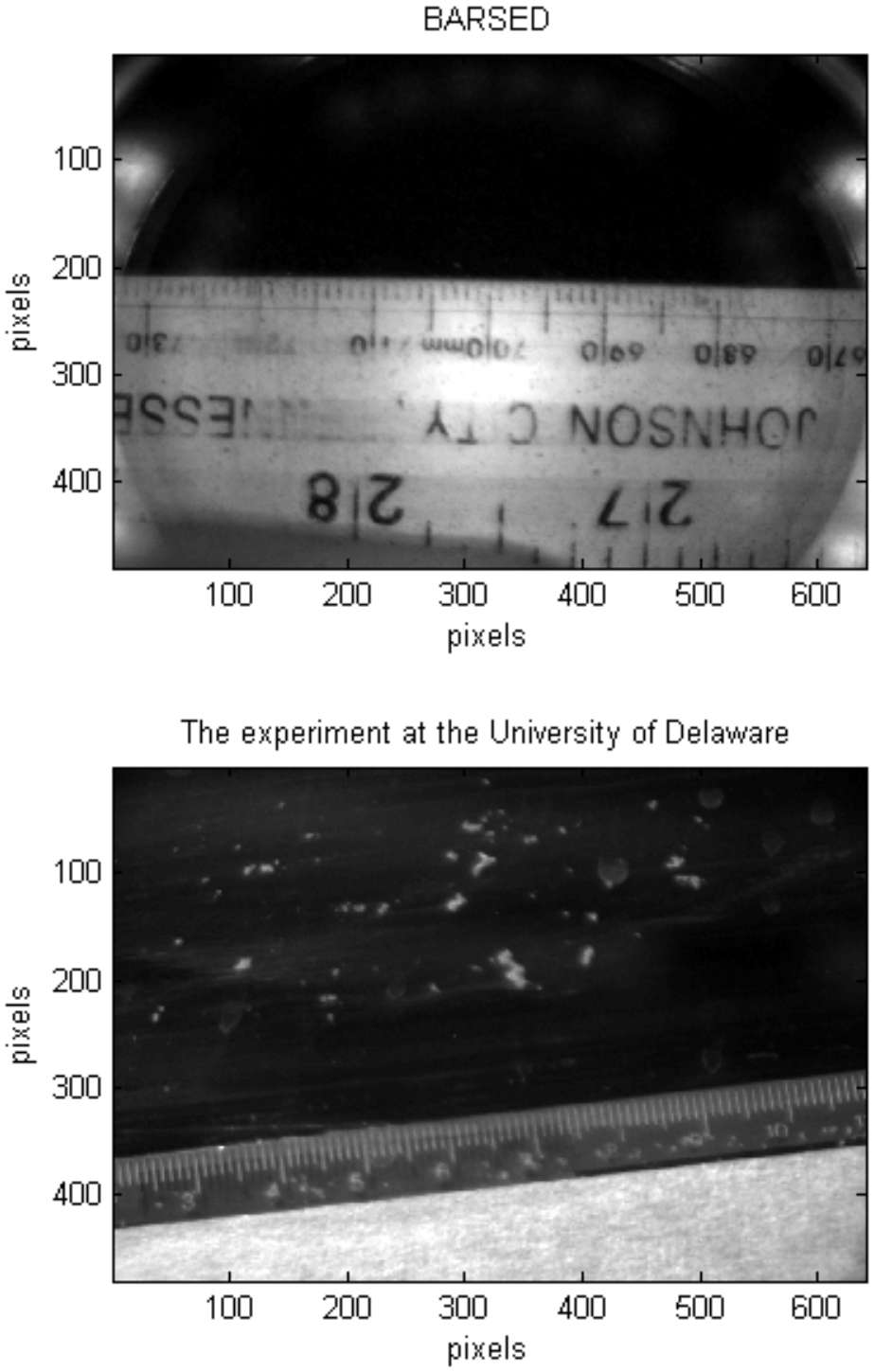

Figure 13. Calibration images for BARSED (top) and the experiment in the CACR (bottom) with the ruler lying parallel to the sediment slope.

3.3.2 The Application of Particle Image Velocimetry

One of the driving interests motivating this work is the development of velocity profiles which extend into the immobile bed. Therefore, vertically dense velocity profiles are most useful. Of special importance are the regions for which the Vectrino II lacks measurements. Combined with the knowledge that flow is predominantly in the cross-shore direction, this interest guided the formation of non-square interrogation windows and search areas. The vertical Interrogation and Search Lengths were smaller than their horizontal counterparts. Counterbalancing the advantages of a dense velocity field are the concerns of over-smoothing. The grid point spacing was set as half of the interrogation window, keeping overlap at 50 %, common for PIV applications.

The selection of search window sizes depended on theory, expectations of the flow field, and trial and error. In the experiment, the velocity was not expected to exceed 2 m/s. For the experiment in the CACR, search lengths s_x of 50, and s_y of 20 pixels were selected. For the experiment at BARSED the search lengths were s_x of 75 and s_y of 30 pixels. The difference in search length results from the difference in pixel per mm scale.

The development of interrogation windows relied on trial and error. The grain-diameter gave some insight. At the experiment in the CACR the average grain diameter was on the order of 1 mm, which translates to 7.5 pixels. As grain boundaries provide substantially more meaningful correlations than grain interiors, capturing grain boundaries within the interrogation window is critical. Furthermore, simple variations in shape of sediment grains provide inadequate distinction with the camera resolution. Therefore, several grain boundaries must be captured, so that the PIV can match grain boundary patterns, resulting in more unique interrogation windows, which

more reliably select the true displacement. Considering this, the smallest interrogation window used was 31 by 17 pixels. The main analysis used an interrogation window of 41 by 21. As stated previously, the asymmetry of the *x* and *z* interrogation lengths is used to better capture velocities near the immobile bed.

3.3.3 Vector Correction

3.3.3.1 Vectrino II Velocity Correction

Raw Vectrino II data contains three major sources of error in the swash zone. Sheet flow, bubbles, and high sediment concentrations can adversely affect acoustic signal propagation. The correlation values from the Vectrino II entirely remove these erroneous velocities. A velocity recorded with a timestamp matching a low correlation value is erroneous. Velocities with correlations below the minimum are replaced with non-numbers (NaNs). This work uses a minimum correlation of 60 %. The second source of error arises because the Vectrino II cannot measure unless submerged. Data collected before the Vectrino II is submerged and after it emerges are not valid. The water depth at the Vectrino II is determined, by collocating the UDM with the Vectrino II. Data is replaced with NaNs whenever the water level is below the height of the Vectrino II. Additionally, the Vectrino II cannot measure velocity in the sediment bed. Any bins below the bed level are replaced with NaNs. An example of the correction process is shown in Figure 14.

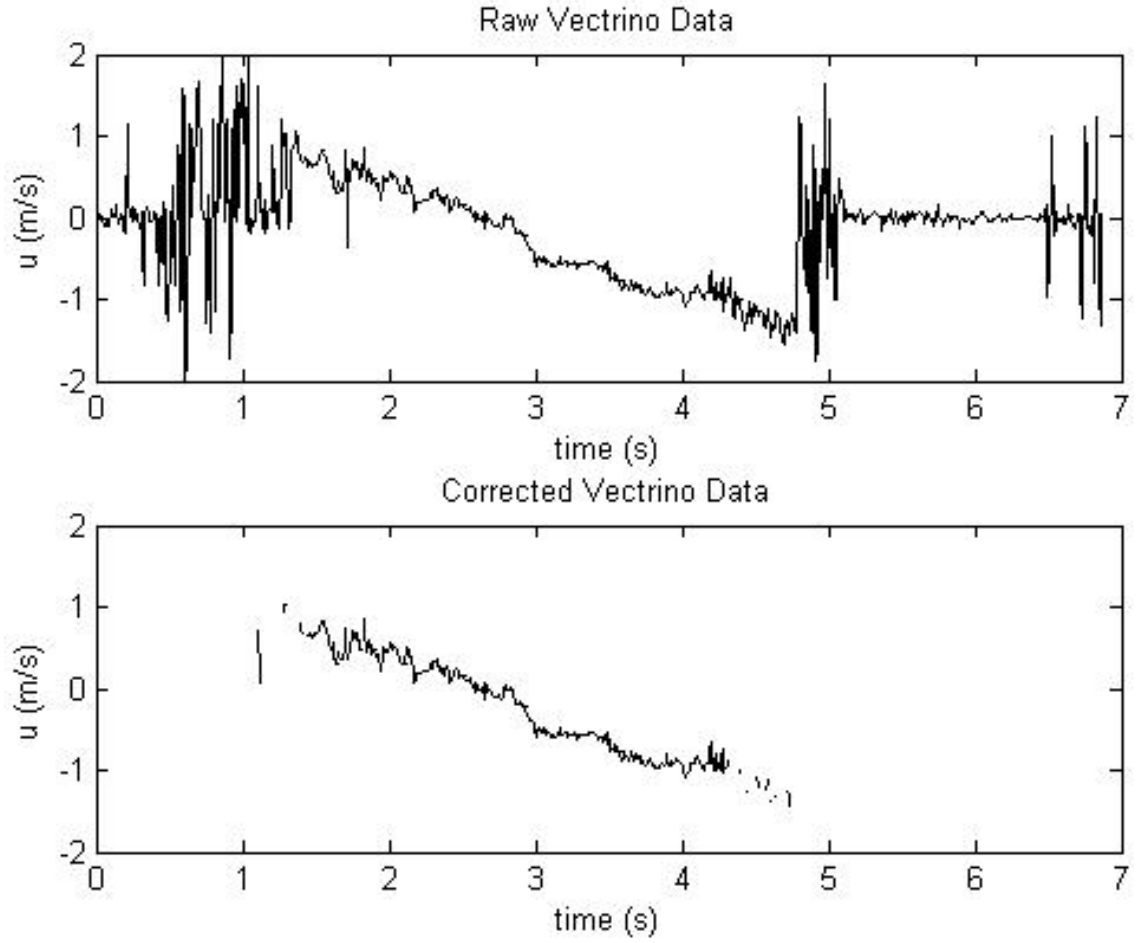

Figure 14. Velocity time series for a single Vectrino II bin, raw Vectrino II velocity (top), corrected Vectrino II velocity (bottom)

3.3.3.2 PIV Output Correction

The most significant problems with output from the PIV come from spurious vectors. The incorrect magnitude and direction misrepresent the flow. With the large number of data points considered in one swash event, the presence of vectors which are independent from the flow conditions distort comparisons and distract from the actual data trends. The removal of spurious vectors forms an important part of PIV

data analysis. Each of the PIV data sets was passed through a series of tests to remove spurious vectors.

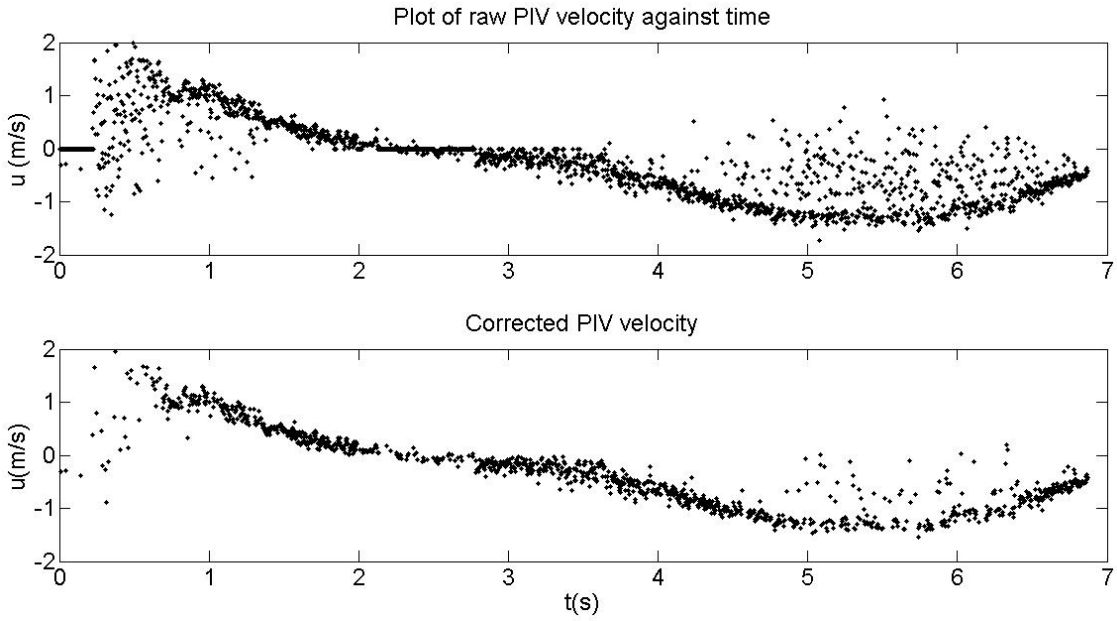

Figure 15. An example of the spurious vector removal process results for the plot of velocity against time for a single elevation, raw data (top), retained data (bottom).

The correction displayed in Figure 16 is the result of four filters. Errors are uncommon enough that most do not border another spurious vector. As a result, in Figure 16, spurious vectors appear as outliers when considered against the data in the time series. The correction process is focused on removing outliers. While not outliers, points with zero velocity do not contribute useful information, and distort comparisons with the Vectrino II. For the first correction, PIV outputs of zero were replaced with NaNs.

In the second step, the approximate time derivative of velocity was examined. The forward difference method was used to approximate acceleration using the data from the velocity time series (Figure 16).

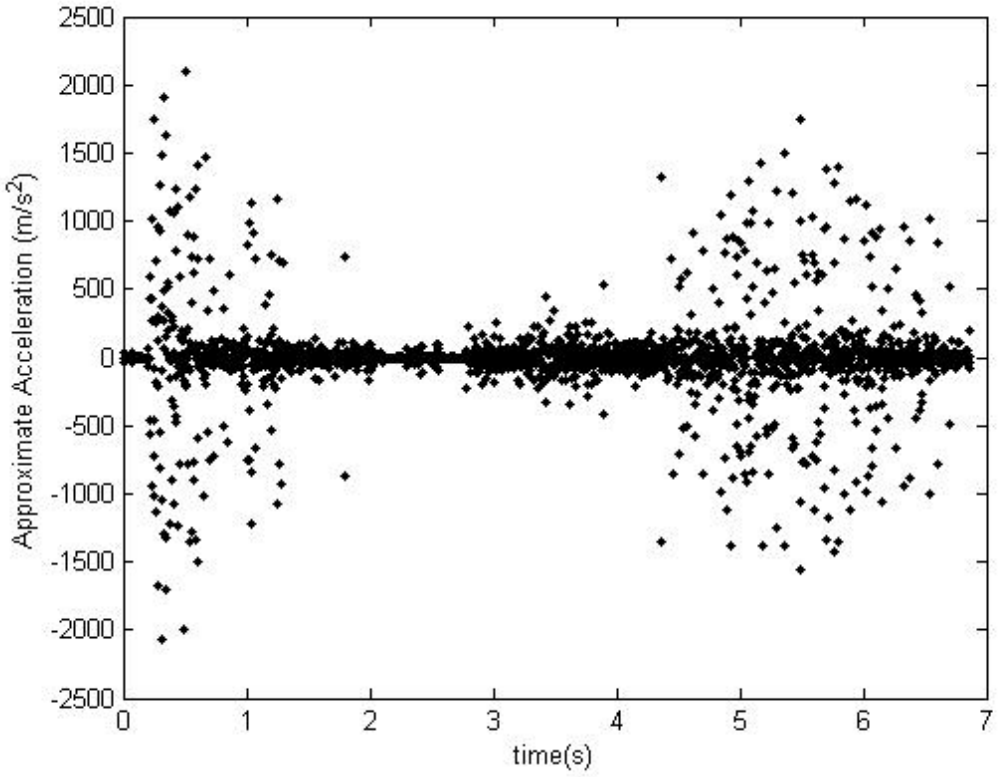

Figure 16. A plot of the approximate acceleration against time at a single elevation.

Unless multiple outliers are clustered together at similar magnitudes, the spurious vectors will appear to have large accelerations. To remove them a cutoff was applied to the magnitude of the plotted acceleration (Figure 16). Each acceleration that exceeded one half of a standard deviation from the mean was removed. Unfortunately,

strictly applying a cutoff removes a minimum of one valid velocity per spurious vector. The acceleration plot in Figure 16 appears largely symmetric because the velocities before and after a single outlier are similar. Therefore the difference between a correct velocity and an outlier will be large, and the correct velocity will also be removed. The spurious vector will be removed if the velocity then returns to the trend, causing a second large apparent acceleration. Additional effort will be required to improve data quality control using the acceleration as a criterion.

The third test removed velocities farther than 20 % from the average velocity of the surrounding 8 points in time at the same elevation. Given the small time step, the variation in velocity over 9 time steps is unlikely to be large. The fourth test removed all points with different signs than the 9 velocities before and after.

3.3.4 Data Alignment

Given the temporally and spatially dynamic nature of the flow considered in this work, spatial and temporal synchronization is critical for comparisons between the sensors and camera.

3.3.4.1 Temporal Alignment

Matching times is the simpler of the two alignments. As all of the elements were connected to the same time server, the timestamps associated with each datum are comparable. The data frequency rates were 301Hz for the camera, 100 Hz for the Vectrino II, and 8 Hz for the UDM. All of the data were interpolated to 301 Hz. One potential problem with the camera collection frequency was that this application could not access the specific timestamps associated with each image. As a result, collection was assumed to fit 301 Hz exactly. The time elapsed between images may have varied

on the order of 0.2 ms. While the impact of this temporal uncertainty was not investigated; the assumption was made that it will have negligible effect on the analysis.

3.3.4.2 Spatial Alignment

The Vectrino II was placed at the same approximate cross-shore location as the camera, near the alongshore median of the flume, elevated approximately 60 mm from the bed. For the data collected in the CACR, cross-shore pixel position of the Vectrino II can be approximated from the imagery. The sensor head can be observed in the imagery, centered at approximately 400 pixels to the right (Figure 17).

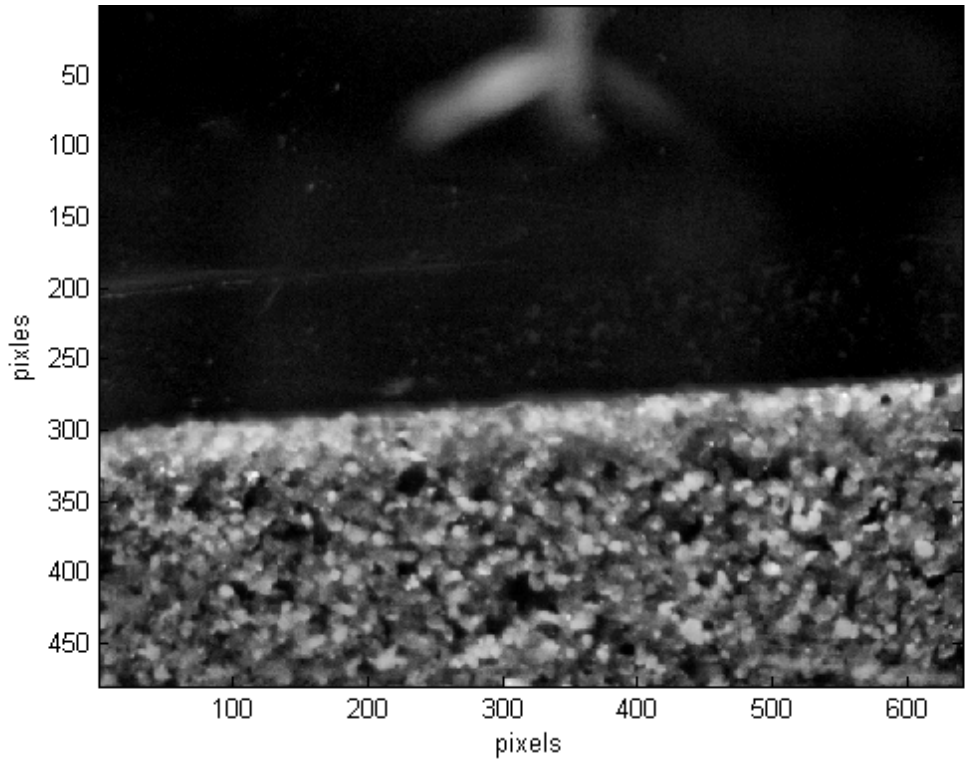

Figure 17. A frame collected before the first run (CACR experiment), indicating the cross-shore location of the Vectrino II.

The three dimensional shape of the field of view from the camera is conic, making the horizontal location of 390 pixels coincide with different cross-shore positions for different cross-shore/vertical planes. The alongshore difference between the plane of the flow field which the camera examined and the position measured would make the Vectrino II appear seaward of its true location in the imagery. However, this distortion is considered small when compared to the accuracy of the alternative assumption that the Vectrino II was centered in the field of view.

The pixel height of the bed in the first frame before the occurrence of the first swash event was measured at the cross-shore pixel location of the Vectrino II as 287 pixels. Using the measured pixel to meter scale the approximate pixel locations of the Vectrino II velocity measuring locations were determined. The accuracy of the height estimate for the Vectrino II combined with the possibility of alongshore bathymetry variation was on the order of 3 mm. The offset was selected to minimize the relative error between the Vectrino II and PIV. Through this comparison, an offset of 2 mm was added to the Vectrino II height, bringing it to 62 mm above the sediment bed.

In the data from BARSED, the position of the Vectrino II and camera were less accessible, so their relative vertical positions were not specifically measured. The position of the bed was found with a code examining the amplitude of the beam which the Vectrino II sends to determine the bed level (code provided by Ryan Mieras). The Vectrino II happened to have no bins beneath the bed, so no corrections for the bed level were needed.

Chapter 4

Results and Discussion

4.1 Discussion of Results from the Experiment in the CACR

4.1.1 Velocity Time Series from the Experiment in the CACR

The results presented in this section compare the velocity measurements from the Vectrino II with the estimates from PIV at a single cross-shore location, across the entire swash event.

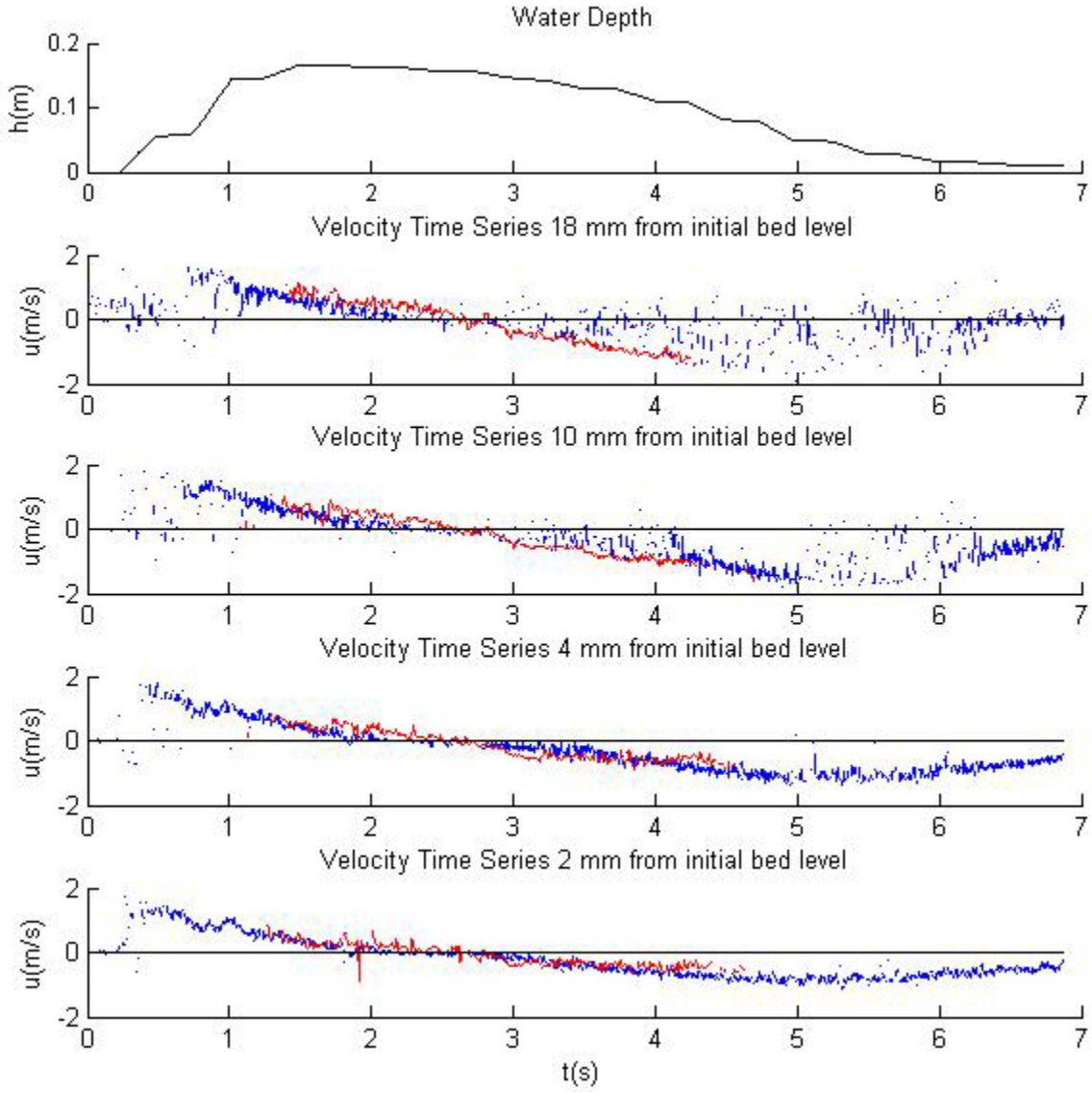

Figure 18. Time Series comparison between the velocities measured by the Vectrino II (red), and those from PIV (blue) from 18 to 2 mm from the initial bed level.

A clear relationship is visible between elevation and density of PIV velocities after correction. Lower elevations have more consistent trends, extend earlier, and have smaller gaps around flow reversal. This is most likely related to PIV dependence

on sediment concentration, and the variation in sediment concentration with elevation. Each interrogation window must contain a pattern which is unique to the search region. As most sediment grains will appear to be similar in the imagery, unique patterns of sediment must be captured for PIV to yield a valid velocity.

One interesting feature of the velocity time series from 4 mm and 2 mm is that they always over-estimate towards the end of the Vectrino II measurements in the backwash. The most probable cause is sheet flow.

4.1.2 Error

In order to address the issue of error, PIV velocities must be quantitatively compared with measurements from the Vectrino II. The velocities which passed through both corrections were compared. The relative error may be represented as

$$\%\, error = \left|\frac{u_V - u_P}{u_v}\right| \cdot 100\% \quad (3)$$

where u_V is the Vectrino II velocity and u_P is the PIV velocity, both for the same location at the same time.

These relative errors were averaged across time for each elevation. The error was calculated for all interrogation window sizes tested.

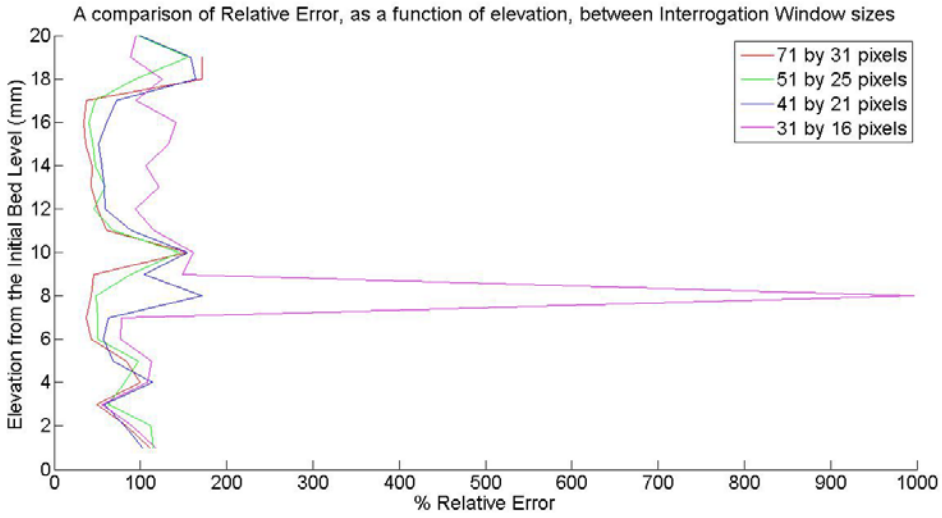

Figure 19. Relative error as a function of elevation, for all interrogation window sizes from the experiment in the CACR.

Examining the plot of relative error as a function of elevation (Figure 19) it is evident that above the 6 mm, the 31 by 16 pixel interrogation window is most inaccurate. To provide a more descriptive representation of error, Figure 19 is plotted with this interrogation window size omitted in Figure 20.

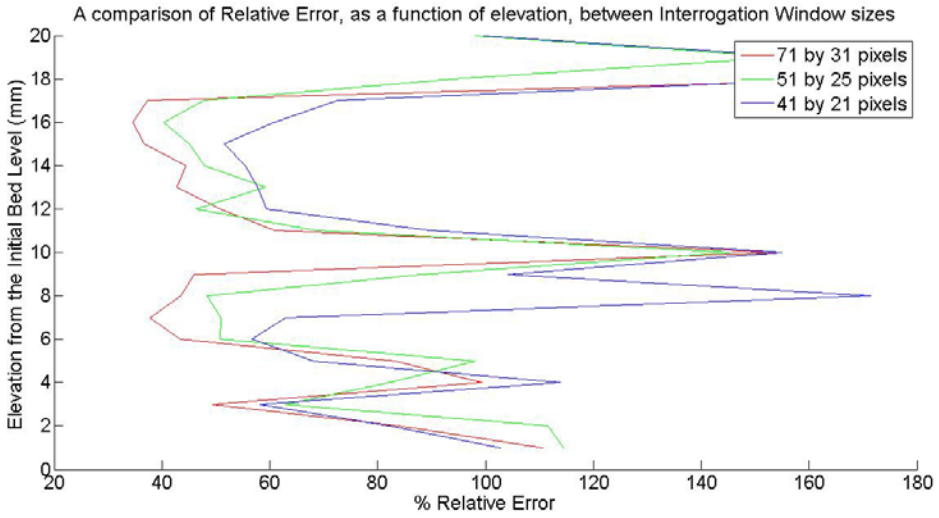

Figure 20. Relative error for the larger three interrogation window sizes from the experiment at the in the CACR, as a function of elevation.

All three of the larger interrogation windows give similar results (Figure 20). Weighing this information against the intention to resolve the large velocity gradient in the sheet flow layer an interrogation window size of 41 by 21 pixels was selected for the following results and discussion presented. Without applying a more refined correction the PIV data will have very large relative errors when time-averaged across the entire swash event. To elaborate further on the variation in error, time series and histogram representations of relative error are provided at various elevations.

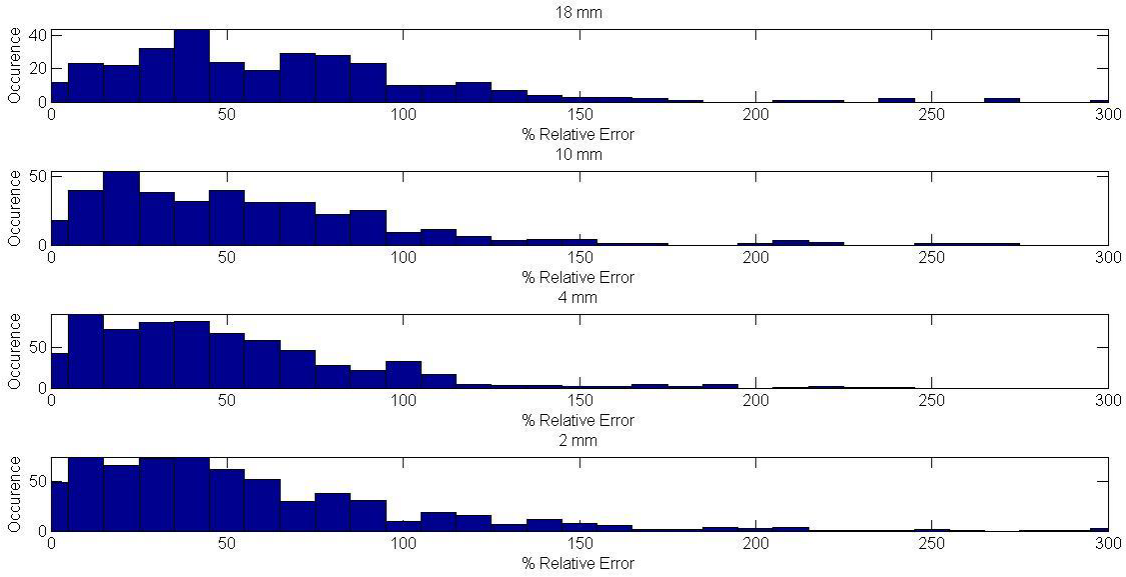

Figure 21. Histograms of the relative error for the velocities at elevations of 18, 10, 4 and 2 mm

The histograms for the relative error of the PIV velocities display several important trends. They are all asymmetric. As the height decreases, the median of the histograms grows smaller, reflecting improvement in the error for many of the velocities. The significant difference between the time-averaged relative errors (Figure 20) and the median from the relative error histogram (Figure 21) suggests the importance of a more robust and descriptive error analysis technique. Additionally, the spatial alignment includes the potential for error, which would magnify the relative error of the velocity. The high errors are particularly surprising given the clear trend of the PIV results and its apparent similarity with the Vectrino II velocities.

4.1.3 Vertical Velocity Profiles from the CACR

Using both Vectrino II data and the results of Particle Image Velocimetry for the camera imagery, vertical velocity profiles were developed for a single swash event.

The following Figures present frames from the imagery of the swash event, with the vectors from the Vectrino II and those generated by PIV overlaid on the corresponding image. Water depth is also shown to provide context. The vertical lines on the water depth plot indicate the corresponding times. While no sediment concentration data were collected, qualitative insights may be visually inferred about comparative sediment concentration and the modes of sediment transport, particularly the occurrence and thickness of sheet flow.

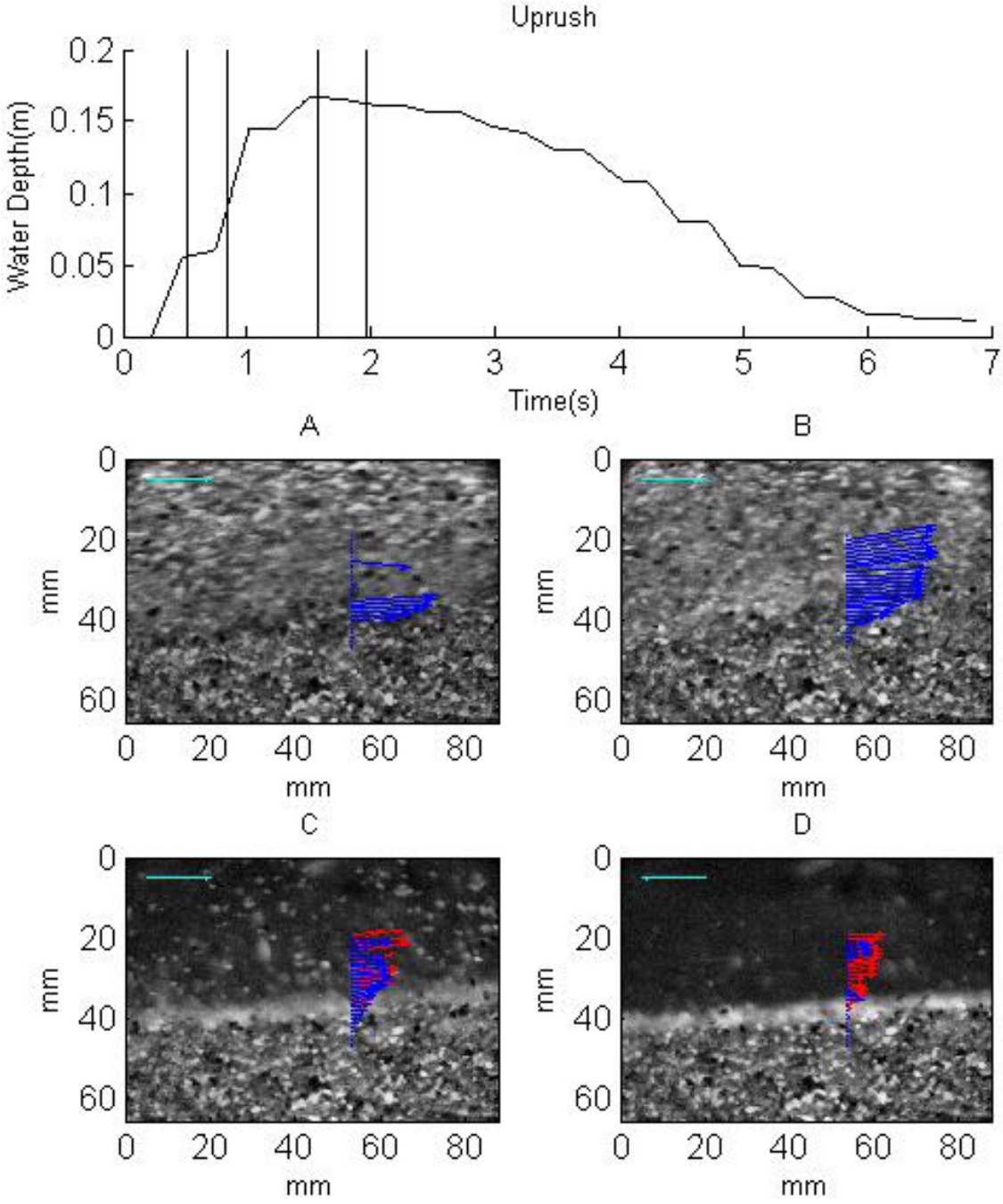

Figure 22. Water depth (top) and image frames from the uprush in the CACR experiment, PIV (blue), Vectrino II (red), 1 m/s scale vector (cyan)

Frame A portrays the flow shortly after the arrival of the collapsed bore. The Vectrino II cannot measure, and PIV only determines a velocity estimate in the sheet flow layer. Higher up, the flow is faster, lower concentration, and more turbulent, so PIV is unable to return valid velocities. This is likely due to motion induced image distortions. The image clarity markedly decreases above 40 mm, as sediment grains merge and grain boundaries loose clarity. One of the works foci is developing velocity profiles in sheet flow, so the velocities displayed in frame A indicate the satisfaction of the goals: determining velocities earlier in uprush than the Vectrino II, and determining sheet flow velocities. This is less than half of a second since the start of uprush, and continuous measurement of a velocity profile in uprush sheet flow has begun. To put the significance into context, the Vectrino II does not measure any velocities for another second.

In frame B, PIV estimates a full velocity profile including sheet flow and suspended load. Sediment concentrations and velocities are high, but lower than those in frame A. This is still before the Vectrino II has made any velocity measurements.

Frame C shows the introduction of Vectrino II measurements. Sheet flow is no longer mobilized and suspended sediment concentrations are lower. The velocity profiles agree over the lower 20 mm of the water column, but above that the PIV consistently provides lower results. The Vectrino II, on the other hand, provides a full velocity profile.

Frame D captures a span of the uprush with low sediment concentrations. PIV is incapable of determining accurate velocities due to insufficient patterns of moving sediment. The few vectors which survived the spurious vector removal should be

removed with a more robust removal algorithm. At this stage in the uprush the Vectrino II collects a full velocity profile.

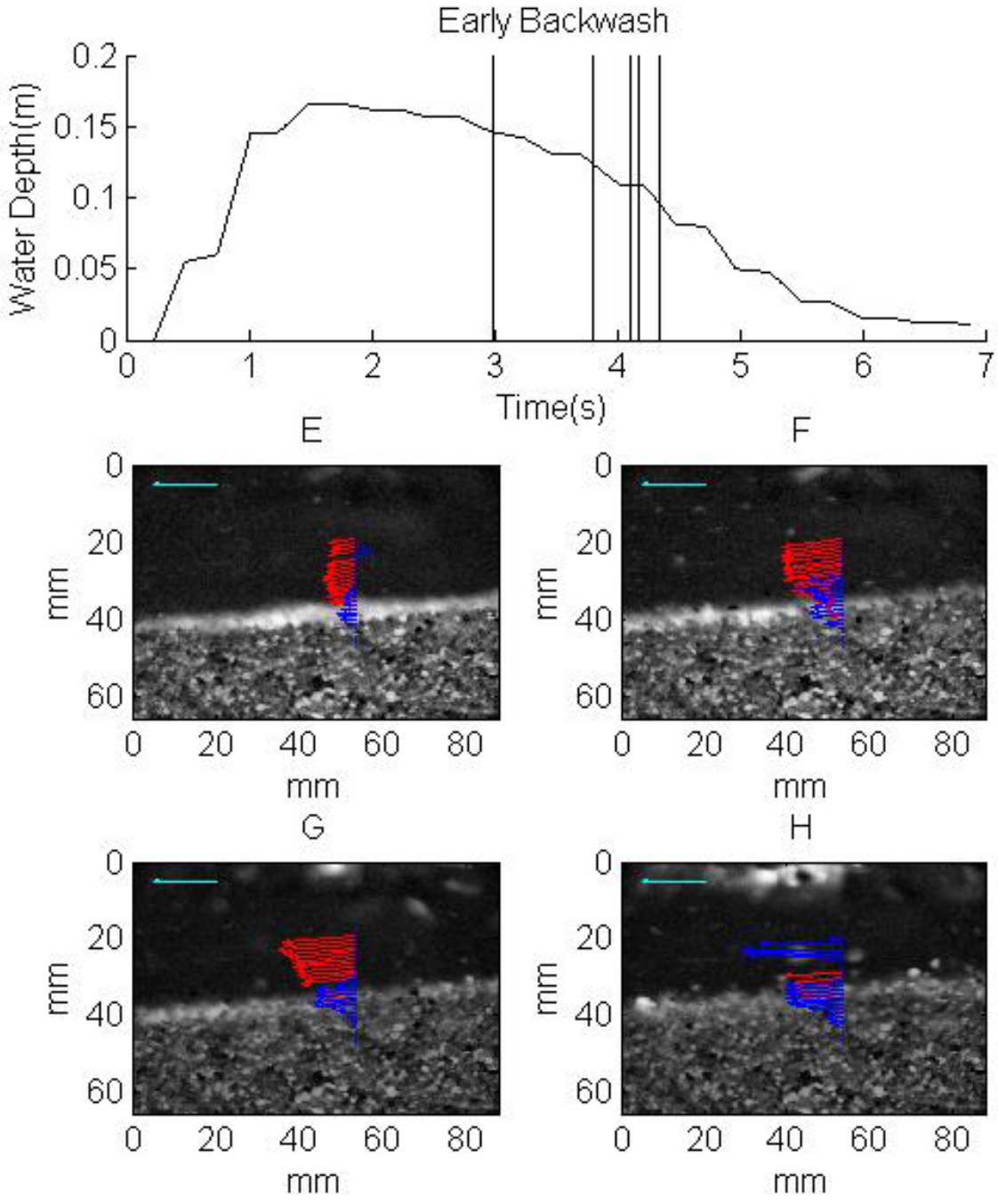

Figure 23. Water depth (top) and image frames from backwash, before significant sediment mobilization, PIV (blue), Vectrino II (red), 1 m/s scale vector (cyan)

Frames E, F, and G show a temporal span over which the Vectrino II develops full velocity profiles. Between frames E and G the PIV results display an informative trend. The region for which PIV determines credible velocities grows with sediment concentration. The flow in frame E has low enough sediment concentrations that PIV lacks substantially robust patterns to match outside of the first few mm of flow. As sediment concentration in the water column increases with time, the velocity profiles which PIV develops improve, growing to approximately 10 mm and containing more consistent velocities.

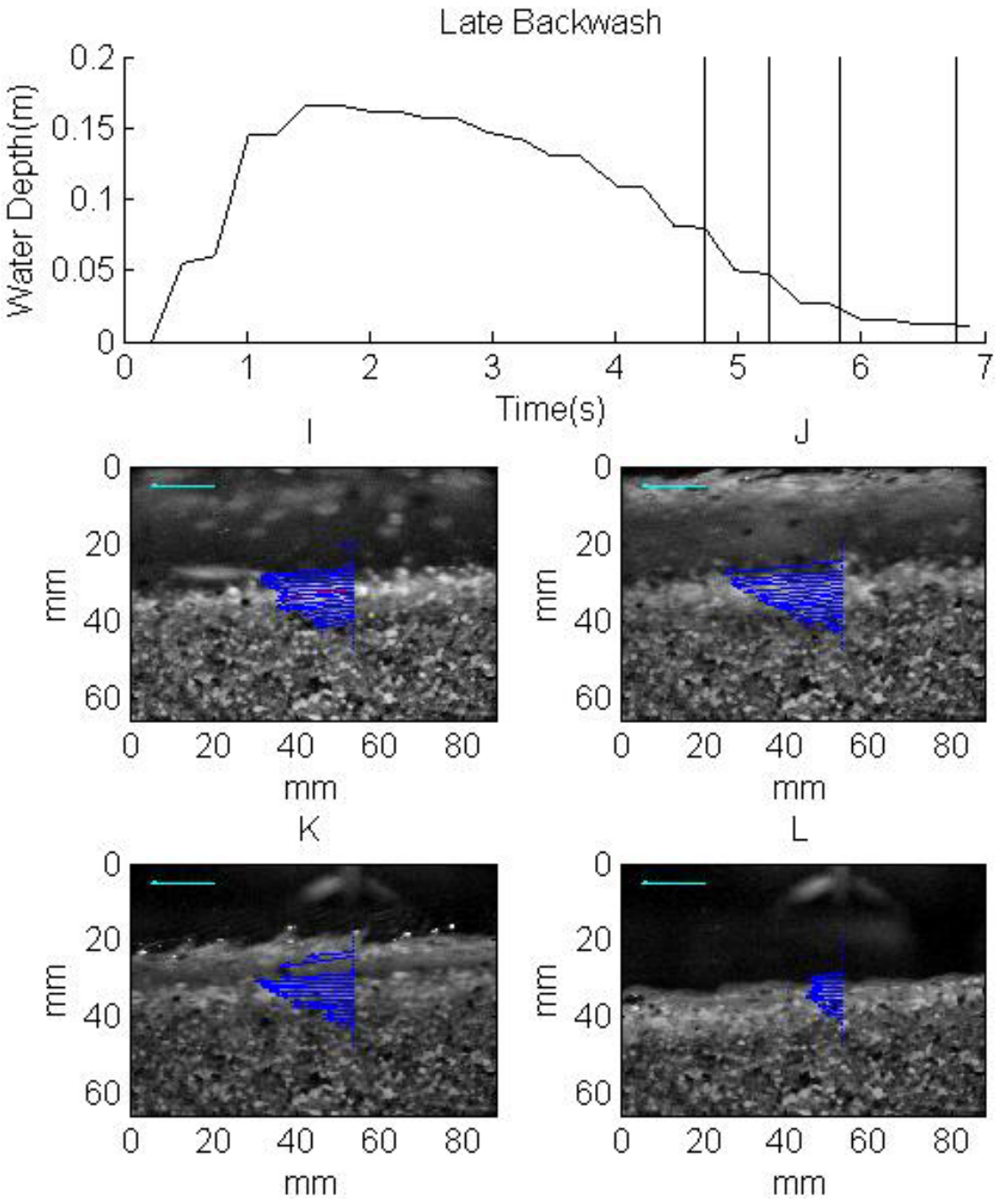

Figure 24. Water depth (top) and image frames of late backwash from the experiment in the CACR, PIV (blue), Vectrino II (red), 1 m/s scale vector (cyan)

Frames I and J continue the trend of the PIV results in frames E to H. The backwash is accelerating, resulting in thicker sheet flow, and a wider region of valid PIV velocities. In the decelerating backwash (frames K and L) the sheet flow thins. PIV provides a credible velocity profile through the sheet flow layer. The Vectrino II measures poorly in frame I and is no longer submerged for frames J, K, and L.

4.2 Results from BARSED

For the data from BARSED, a single selection from the imagery was analyzed. The sample is from series of monochromatic waves with a period of 7 seconds and a height of 0.4 m at the wave-maker. It was selected because of its particularly continuous Vectrino II data. Because the region considered was just outside of the swash zone, the Vectrino II was never exposed, allowing for a longer comparison. The Vectrino II data matches the PIV data particularly well.

4.2.1 BARSED Velocity Time Series

The following section presents the times series of velocity from BARSED at various elevations.

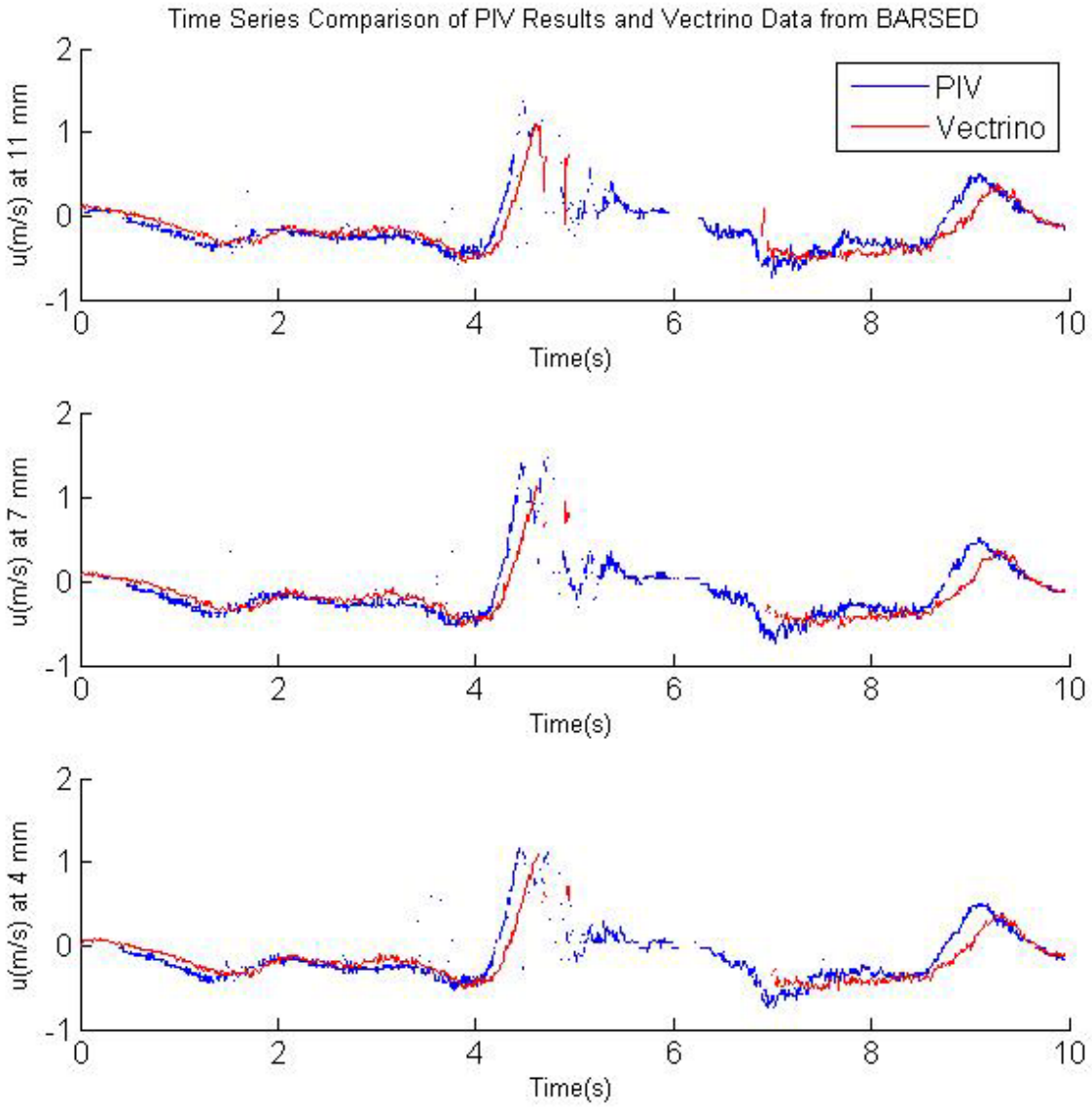

Figure 25. Comparisons of Velocities at 11, 7, and 4 mm above the bed plotted against time, PIV (blue), Vectrino II (red)

The velocity profiles from BARSED display a trend which is incompatible with the assumptions made. The red line is the Velocity measured by the Vectrino II, and the blue line is the output from PIV. This is problematic because the PIV yields

higher magnitude velocities at all four locations. . Around 4.5 and 9 seconds into the selection the PIV very clearly estimates a faster velocity. Points in time where self-consistent velocity trends are opposing signs indicate that the difference is not simply the result of an erroneous scale. Both techniques lose the end of uprush but capture the beginning, under these conditions. The finer grained sediment resulted in a smoother PIV velocity time series than the course grained sediment. The long stretches of similar PIV and Vectrino II velocity provide validation for the PIV results.

4.2.2 Error

Quantifying the error associated with the PIV results was approached in a similar fashion to the method used for the data from the CACR. Relative errors were determined at every point, for every timestamp. In contrast to the strong agreement between the velocity time series trends, when averaged across the entire time span, the error is substantially larger than the data from the experiment in the CACR.

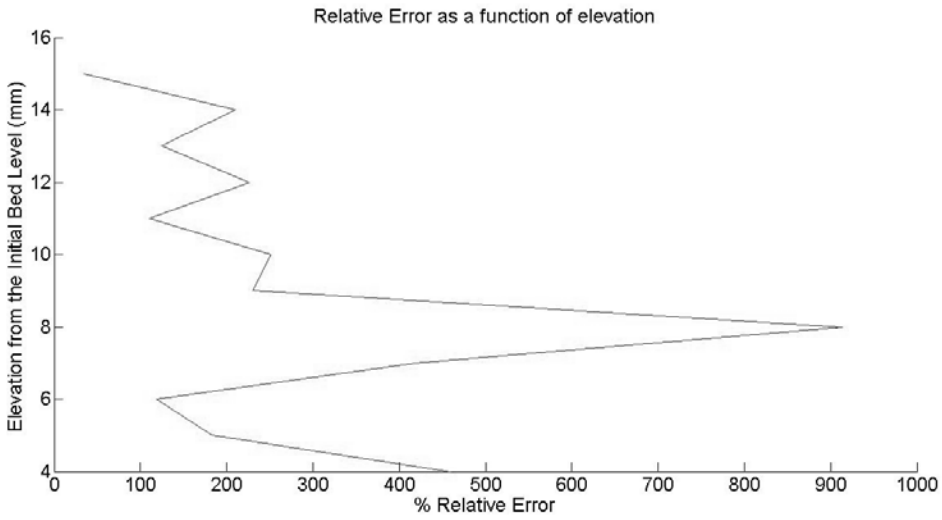

Figure 26. Relative Error between PIV and Vectrino II data from BARSED

The time-averaged relative errors for the data from BARSED (Figure 26) are nearly 200% larger than those from the experiment at the CACR (Figure 20). Given the remarkable similarity of plots in figure 25, more information is needed to address the methods error. The histograms in figure 27 provide more insight into the error associated with the PIV results.

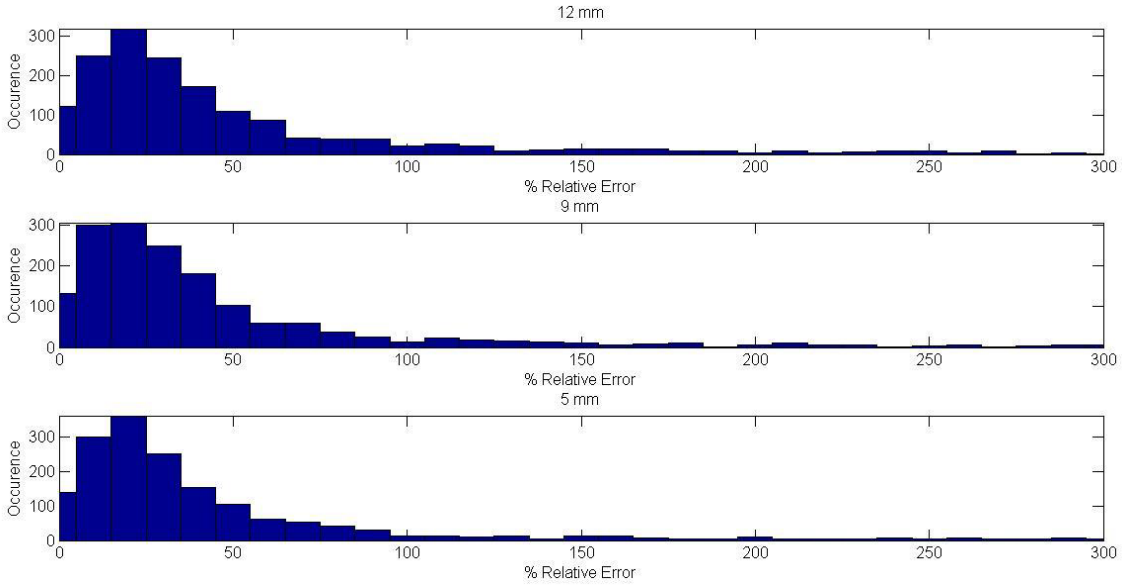

Figure 27. Relative error histogram for 12, 9, and 5 mm velocities at BARSED

Comparing Figures 26 and 27, the time-averaged error is also misleading for the BARSED data. The histograms in Figure 27 are significantly asymmetrically skewed low; therefore the time-averaged error is biased by outliers. Figure 27 shows a lower grouping of errors than Figure 20 for the coarser grained sediment. The data from BARSED matches the velocity estimates more closely over a significant portion of the sample, which is displayed in the histogram data (Figure 27).

4.2.3 Vertical Velocity Profiles from BARSED

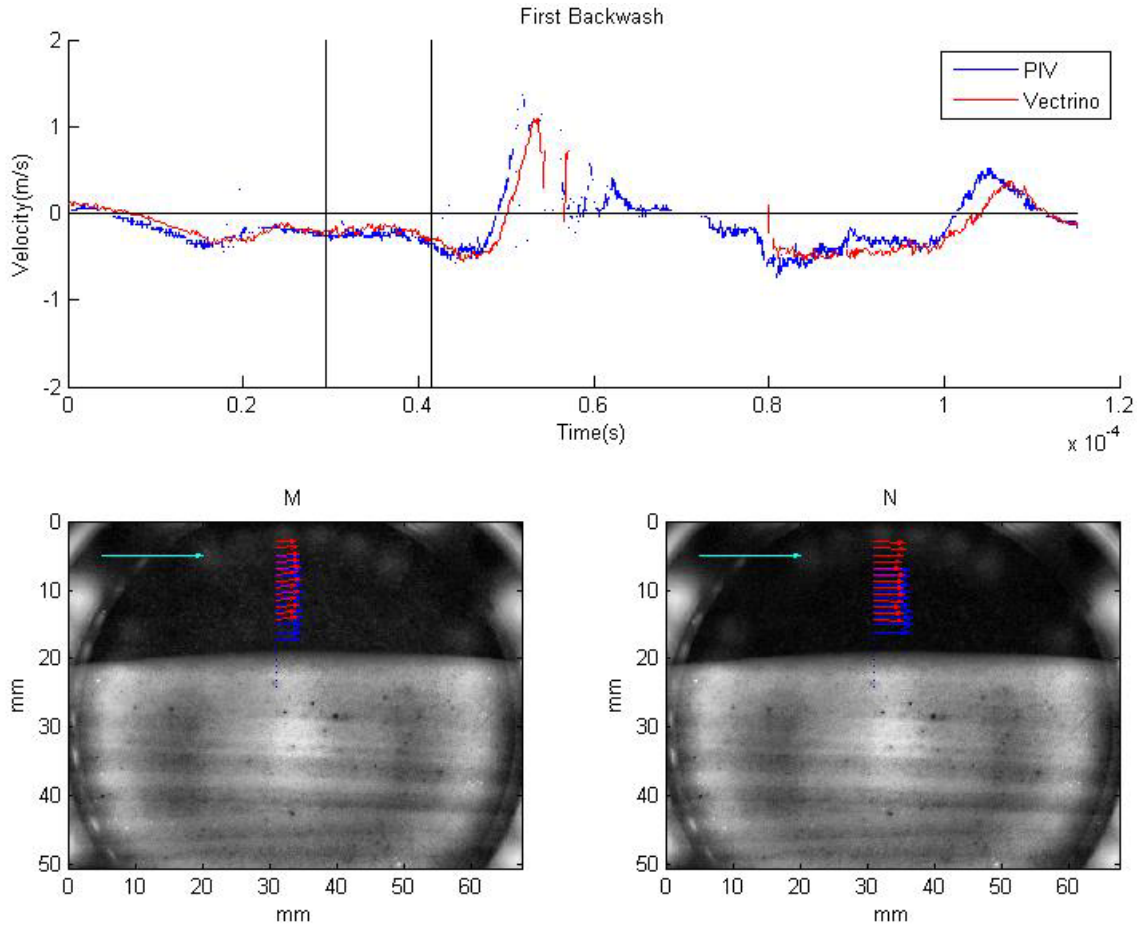

Figure 28. Velocity time series (top) image frames for the first backwash considered from BARSED, PIV (blue), Vectrino II (red), 1 m/s scale vector (cyan)

In frames M and N, depth uniform profiles of backwash velocity are similar between PIV and the Vectrino II. Frames M and N show that, over most of the water column, PIV with finer grained sediment can resolve velocities accurately.

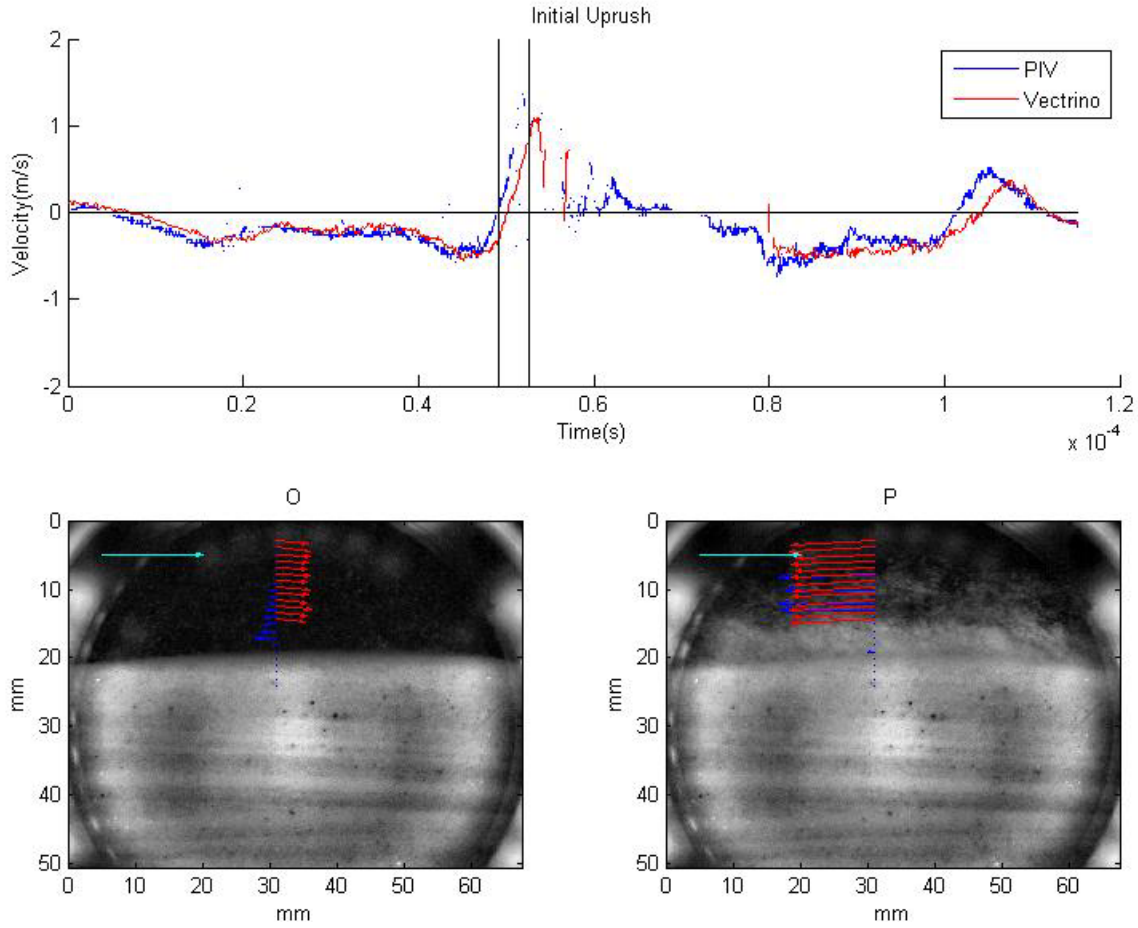

Figure 29. Velocity time series (top) image frames for the initial uprush considered from BARSED, PIV (blue), Vectrino II (red), 1 m/s scale vector (cyan)

Frame O shows the transition from uprush to backwash occurring at different times between PIV and the Vectrino II. While PIV has already reversed directions, the Vectrino II is still depth uniform. Based on the consistency of the velocity profiles in frame O and the similarity between the two techniques over the long time span typified by frames M and N, it is unlikely that either technique is incorrect in frame O. To address the apparent inconsistency the assumption of alongshore uniformity must be recalled. The camera views an *xz* plane immediately adjacent to the camera housing

front and the Vectrino II measures velocity at the sections alongshore median. This indicates slightly non-uniform alongshore bathymetry. Some scour was observed along the wall with the camera, so the same height from the bed would be higher underneath the Vectrino II than the camera, altering when the flow changes direction. Additionally, the assumption of alongshore uniform flow may not be perfectly valid. The substantial agreement between the two techniques over the first backwash indicates that for the majority of the sample, flow is alongshore uniform. Near the transition from backwash to uprush, however, the bathymetry may have introduced alongshore non-uniformities to the flow. This could provide an explanation for the different transitions between backwash and uprush, as well as the different beginnings of uprush between the two techniques.

Frame P displays sheet flow during uprush. PIV is unable to determine any velocities within the sheet flow. This could be result of an overly abrasive spurious vector removal process. Another possibility is that the sediment is too fine with respect to the pixel to mm scale in the imagery. A pixel covers a 0.1053 mm square, and an average sediment grain was approximately 0.17 mm. With motion induced distortions in a fast moving high concentration flow, sediment could certainly blend across the grain boundaries, removing the most robust feature for the PIV to match. Determining the roles different factors played requires further analysis.

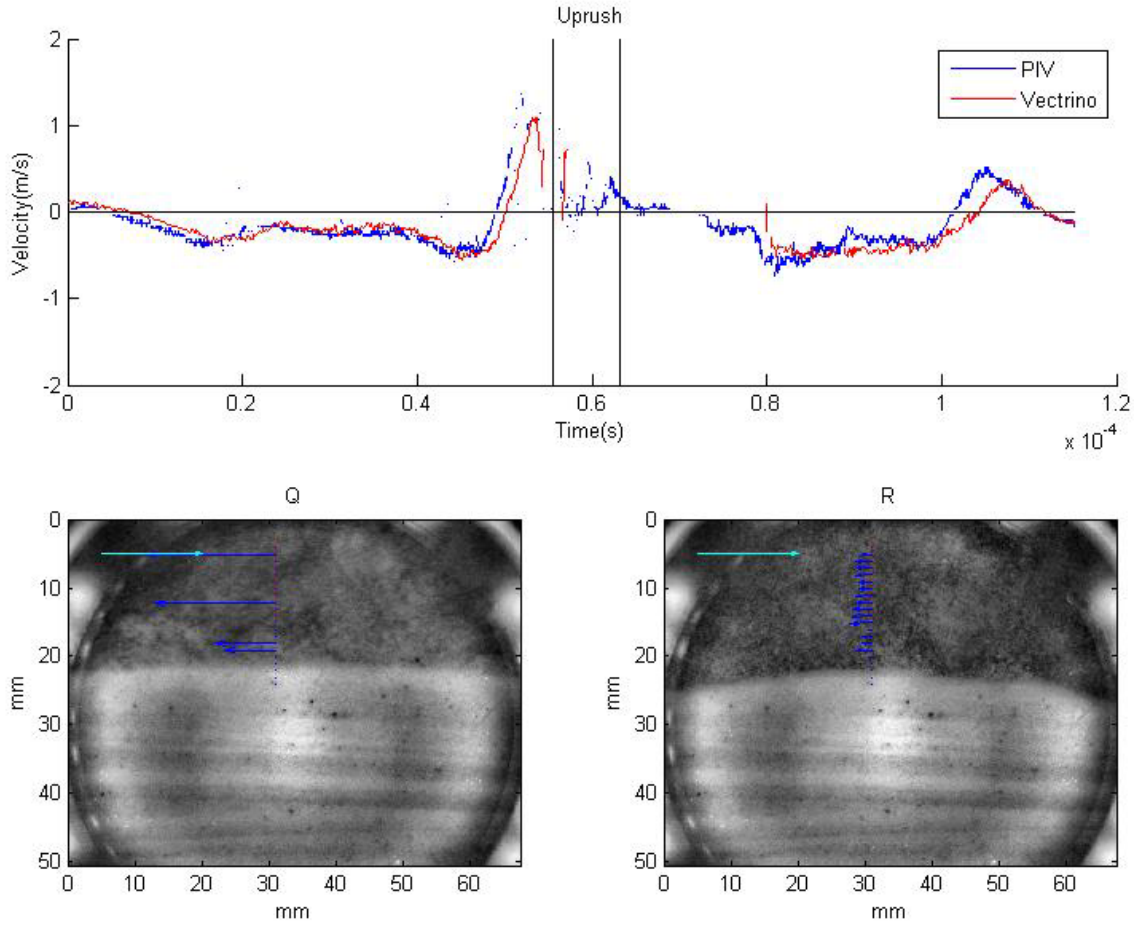

Figure 30. Velocity time series (top) image frames for the uprush considered from BARSED, PIV (blue), Vectrino II (red), 1 m/s scale vector (cyan)

PIV does not determine velocity consistently through the deceleration of the uprush. Velocities which are provided, such as those in frame Q, are sparse. The next full profile of velocity measurements are made near the end of uprush (frame R).

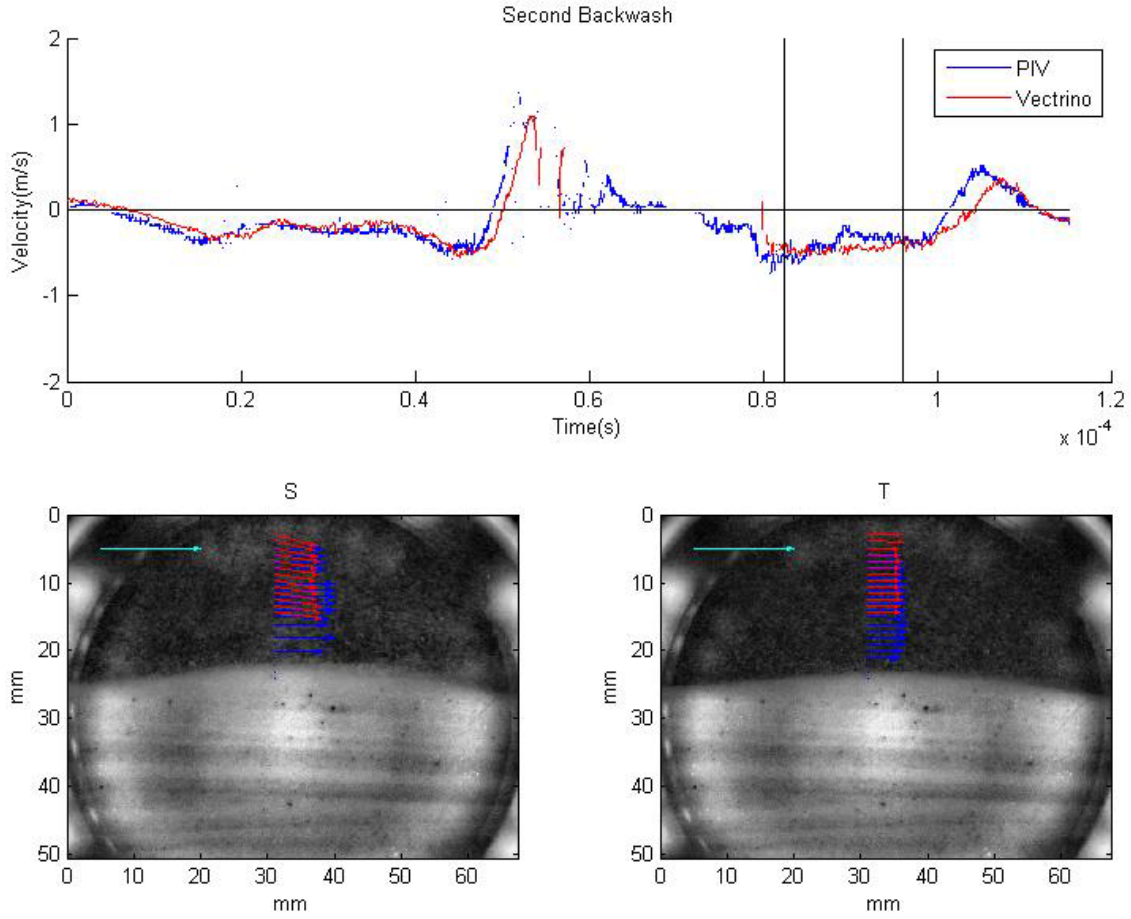

Figure 31. Velocity time series (top) image frames for the second backwash considered from BARSED, PIV (blue), Vectrino II (red), 1 m/s scale vector (cyan)

By frames S and T, both techniques determine similar velocities during backwash. Similar to frames M and N, the velocity profiles are roughly depth uniform. Frames, M, N, S and T show the strong capability of the finer grained sediment to accurately determine velocity. The extensive similarity of the Vectrino II velocity allows for a robust validation of the PIV results.

Chapter 5

Conclusion

This thesis aimed to investigate the ability of particle image velocimetry to determine vertical velocity profiles through the sheet flow layer, at the beginning of uprush, and the end of backwash. Between the two experiments, the various aspects of these goals were satisfied.

The experiment in the CACR determined that PIV can determine sheet flow velocities earlier and later in the swash flow than the Vectrino II could measure. Where sheet flow was observed PIV provided a spatially and temporally consistent vertical velocity profile, beginning with zero velocity and extending through the sheet flow. Velocities were also determined above the sheet flow layer, though over a shorter duration, and less consistently. The difficulty with the validation with Vectrino II data is the contrast in regions of strength. For the coarse grained sediment, PIV provided the best trends in the first 2 s and last 3.5 s. The Vectrino II measures best between roughly 1.5 s and 4.5 s. The regions in which both sensors perform optimally are only the 0.5 s from 1.5 to 2 s in the uprush, and the 1.0 s between 3.5 and 4.5 s in the backwash. This limits the potential for validation with time-averaged error. The experiment in the CACR does answer the question of whether PIV is capable of resolving velocity in the sheet flow layer, as the vertical velocity profiles and velocity time series show.

BARSED determined that PIV can develop accurate vertical profiles of velocity in a swash event. The long periods of time between the first and second

uprushes in the sample validate the results from PIV. The velocities from PIV indicate that PIV loses quality for high concentrations of finer grained sediments, such as during the initial uprush and during sheet flow.

Perhaps the largest area of improvement for considering this data would have been the application of a more refined spurious vector removal, and a more refined consideration of error.

As the finer grained sediment of BARSED satisfied the first point, and the coarse grained sediment of the experiment in CACR satisfied the second, it appears that the capabilities of PIV at determining velocities in the swash zone are tied to sediment size. In order to achieve both goals in the same experiment sediment is likely needed with an average grain size between the 1 mm and 0.17 mm sediments considered. The two experiments demonstrate that PIV can determine accurate vertical profiles of velocity, as well as velocities which current meters cannot measure.

REFERENCES

Holland, K.T., Puleo, J.A., and Kooney T.N., 2001. Quantification of swash flows using video-based particle image velocimetry, Coastal Engineering 44, 65-77.

Komar, P. D., 1978. Relative Quantities of suspension versus Bed-Load Transport on Beaches. Journal of Sedimentary Petrology 48 (3), 921-932.

Roth, G., Hart, D., Katz, J., 1995. Feasibility of using the L64720 video motion estimation processor (MEP) to increase efficiency of velocity map generation for particle image velocimetry (PIV). In: Huang, T.T. (Ed.), ASME/JSME Fluids Engineering and Laser Anemometry Conference and Exhibition. American Society of Mechanical Engineers, Hilton Head, SC, 387–393.

Vectrino Profiler. Nortek. Web. <http://www.nortek-as.com/lib/brochures/vectrino-ii>.

7.2 Nearshore Wave Processes Terminology USACE (1992). Digital image. *US Department of Transportation Federal Highway Administration*. FHWA, 24 Sept. 2014. Web. 22 Apr. 2015. <http://www.fhwa.dot.gov/engineering/hydraulics/hydrology/hec25c7.cfm>.

Appendix

VARIABLES

Table

Variable	Description	Dimensions	Units
X	Total Position	Length	m
x,y,z	Position, separated into coordinate components in the cross-shore, alongshore, and vertical	Length	m
U	The magnitude of local velocity	Length/time	m/s
u,v,w	Local velocity separated into coordinate components in the cross-shore, alongshore, and vertical	Length/time	m/s
I	The interrogation window in PIV for a grid point	$Length^2$	$Pixels^2$
i	The interrogation length	Length	Pixels
s	The search length	Length	Pixels
R	The search region examined for a grid point in PIV	$Length^2$	$Pixels^2$
S	The search window in PIV	$Length^2$	$Pixels^2$
Φ	The correlation value between I and S	Dimensionless	unitless